

# **Simultaneous Process and Material Design for Aprotic N-Heterocyclic Anion Ionic Liquids in Post-Combustion CO<sub>2</sub> Capture**

Bo Hong, Luke D. Simoni<sup>1</sup>, Joshua E. Bennett<sup>2</sup>, Joan F. Brennecke, and Mark A. Stadtherr\*

Department of Chemical and Biomolecular Engineering  
University of Notre Dame  
Notre Dame, IN 46556 USA

<sup>1</sup>Current affiliation: The Chemours Company, Wilmington, DE, USA

<sup>2</sup>Current affiliation: Department of Chemical & Biomolecular Engineering, Rice University, Houston, TX, USA

\*Corresponding author: markst@nd.edu

July 6, 2016

## Abstract

Aprotic heterocyclic anion ionic liquids (AHAs) are a promising new class of CO<sub>2</sub> absorbents, with a capacity of one mole of CO<sub>2</sub> chemically absorbed per mole of AHA. By tailoring the substituents on the anion, the AHA properties, in particular the enthalpy of absorption, can be tuned over a wide range. Furthermore, the entropy of absorption can be tuned by tailoring substituents on the cation. This then presents a materials design challenge—What are the optimal AHA properties? This challenge is addressed by incorporating AHAs into a simple process model of CO<sub>2</sub> capture from post-combustion flue gas, and formulating the question as a type of simultaneous materials and process design problem. New absorption isotherm data is presented, over a larger pressure range than studied previously, for a few AHAs, and is used to suggest a simple thermodynamic model for CO<sub>2</sub> uptake, to be used in connection with the process model. The possibility of ionic liquids (ILs) that exhibit a 2:1 CO<sub>2</sub> uptake (two moles CO<sub>2</sub> per mole IL) with a cooperative binding mechanism is also considered, with absorption isotherm data for one such compound presented, together with a corresponding isotherm model. The process model is an equilibrium-based material and energy balance model, which is used to determine flowrates, heat duties, and process conditions that minimize a simple energy usage objective function. The sensitivity of this optimum with respect to various material properties and process parameters is studied, for flue gas from both pulverized coal and natural gas combined cycle power plants. The results provide materials property targets for the identification of new AHA molecules for CO<sub>2</sub> capture, leading to significant reductions in heat requirements relative to conventional amine technology.

## 1. Introduction

Current technology for the chemical absorption of CO<sub>2</sub> is widely regarded as very costly and energy intensive in the context of CO<sub>2</sub> capture from large-volume point sources such as fossil-fuel power plants. Thus, there is significant current interest in the development of new materials for CO<sub>2</sub> capture, and a variety of alternative absorbents and adsorbents have been proposed. Several recent reviews<sup>1-45</sup> of the current technology and proposed alternatives are available. In this paper, we will focus on a particular class of CO<sub>2</sub> absorbents known as aprotic heterocyclic anion ionic liquids (AHAs).<sup>46</sup>

The current standard in the chemical absorption of CO<sub>2</sub> is the use of aqueous solutions of amines, often monoethanolamine (MEA) or “advanced amines” (e.g., tertiary amines,<sup>47</sup> piperazine and derivatives<sup>48</sup> or combinations thereof<sup>49</sup>). For example, MEA is the basis for Fluor’s Econamine FG Plus<sup>SM</sup> process and advanced amines are used in the Shell Cansolv process, both of which have been used as representative CO<sub>2</sub> capture technology in evaluating power plant economics with and without carbon capture.<sup>50,51</sup> For aqueous solutions of amines, one of the well-known issues is the need to heat and evaporate large quantities of water during desorption (stripping) of CO<sub>2</sub> from the absorbent. An attractive alternative in this regard is the use of ionic liquid (IL) absorbents,<sup>52-56</sup> which do not require the use of water, and, because of their exceedingly low vapor pressures, essentially do not evaporate. Several ILs provide strong physical absorption of CO<sub>2</sub>,<sup>57</sup> but the resulting CO<sub>2</sub> uptake is not competitive for post-combustion CO<sub>2</sub> capture conditions. CO<sub>2</sub> uptake can be increased by tethering amines to the IL cation,<sup>58,59</sup> thus providing chemical absorption. These so-called task-specific ionic liquids (TSILs) have the same maximum chemical uptake (0.5 mole CO<sub>2</sub> per mole of absorbent; i.e., 1:2 uptake ratio) as MEA, but there is a large increase in viscosity when CO<sub>2</sub> is absorbed. Gutowski and Maginn<sup>60</sup> have shown using molecular simulation that this viscosity increase is due to the formation of a hydrogen bonding network. Quantum calculations by Mindrup and Schneider<sup>61</sup> have shown that the maximum chemical uptake can be increased to 1 mole CO<sub>2</sub> per mole of absorbent (1:1 uptake ratio) by tethering amino acid functional groups to the IL anion, and Goodrich et al.<sup>62</sup> confirmed this experimentally. However, these amine-functionalized ILs also exhibit large viscosity increases with CO<sub>2</sub> uptake,<sup>62</sup> again due to the formation of a hydrogen bonding network.

This line of investigation has led to the development of AHAs. In this class of IL compounds, the amine functionality is retained in the anion, but is incorporated into a ring structure. This reduces the number of free hydrogens and thus reduces opportunities for hydrogen bonding. The resulting materials exhibit high (1:1) chemical CO<sub>2</sub> uptake, without significant viscosity increase.<sup>46</sup> Moreover, by tailoring the substituents on the anion, the AHA properties, in particular the enthalpy of absorption, can be tuned over a wide range.<sup>63</sup> It has also been shown recently that the entropy of absorption can be tuned by tailoring substituents on the cation.<sup>64</sup> This then presents a materials design challenge—What are the optimal AHA properties? For example, a larger enthalpy of absorption, indicating stronger binding of CO<sub>2</sub> to the AHA, implies greater uptake at a given temperature and thus a lower absorbent circulation rate, but it also implies a larger energy input to desorb the CO<sub>2</sub>. Such tradeoffs suggest that there exists some optimal range of property values. In this paper, we will address this materials design problem by incorporating AHAs into a simple process model of CO<sub>2</sub> capture from post-combustion flue gas. We will present new absorption isotherm data, over a larger pressure range than studied previously, for a few AHAs, and use this to suggest a simple thermodynamic model for CO<sub>2</sub> uptake, to be used in connection with the process model. We will also consider the possibility of ILs (not necessarily AHAs) that exhibit 2:1 CO<sub>2</sub> uptake with a cooperative binding mechanism, presenting absorption isotherm data for one such compound, together with a corresponding isotherm model.

To address the materials design challenge, we will formulate the problem as a type of simultaneous process and material design problem. There are many examples of such problems, in which the material is typically a product<sup>65,66</sup> or some compound (often a solvent) used in the process.<sup>67-71</sup> The result of the material design may be a set of desirable bulk material properties, or may be a set of desirable molecular characteristics or actual molecular structure (computer-aided molecular design). In the latter case, some kind of structure-property relationships must be used, typically a group-contribution (GC)<sup>67,72-74</sup> or quantitative structure-property relationship (QSPR)<sup>75</sup> approach, or some other approach such as statistical associating fluid theory (SAFT) or density functional theory (DFT) that incorporates specific molecular characteristics. For example, simultaneous process and material design of physically absorbing ILs for CO<sub>2</sub> capture has been considered by Pereira et al.,<sup>76</sup> Oyarzúna et al.,<sup>77</sup> and Burger et al.<sup>78</sup> using SAFT-based approaches, and by Chong et al.<sup>79</sup> using a GC-based approach. Also, Hada et al.<sup>80</sup> have

described a DFT-based method that has potential in designing ILs for various applications. Material design results, whether bulk or molecular level, are typically mapped in some way to a group or database of existing compounds, either as a subsequent step or as part of the original problem formulation. For the problem of interest here, namely the simultaneous process and material design of AHAs for post-combustion CO<sub>2</sub> capture, we will seek to determine desirable bulk material properties, since no appropriate structure-property relationships for this new class of compounds is available yet. We anticipate that, given desirable bulk properties, quantum chemical calculations can be used to design appropriate AHA molecules, thus determining candidates for laboratory synthesis and characterization.

In the next section, we will discuss the absorption isotherm models used for CO<sub>2</sub> uptake, including new isotherm data. Then, in Section 3 we will describe the simple process model used for post-combustion carbon capture, and our formulation of the simultaneous process and material design problem. This is followed, in Section 4, by a presentation and discussion of results, mostly in the form of sensitivity studies that consider how energy usage is affected by variations in material properties and process parameters. Finally, in Section 5, we will provide brief concluding remarks.

## 2. Absorption Isotherm Models

AHA ILs exhibit both chemical and physical absorption of CO<sub>2</sub>, as represented by



AHA reacts reversibly with CO<sub>2</sub> to form an AHA-CO<sub>2</sub> complex, and there is also physical equilibrium between CO<sub>2</sub> in the vapor phase and CO<sub>2</sub> dissolved in the liquid phase mixture of AHA and AHA-CO<sub>2</sub>. It is assumed that there is no AHA or AHA-CO<sub>2</sub> in the vapor phase. We will assume that the physical solubility of CO<sub>2</sub> is the same in AHA as it is in AHA-CO<sub>2</sub>. This allows us to determine the uptakes due to chemical and physical absorption independently, as the amount of physical absorption will not depend on the amount of chemical absorption. Thus, the overall CO<sub>2</sub> uptake, denoted by  $X$ , is determined from

$$X = X_{\text{phys}} + X_{\text{chem}}, \quad (3)$$

where the physical and chemical contributions  $X_{\text{phys}}$  and  $X_{\text{chem}}$  are treated separately, as described below. We will express the  $\text{CO}_2$  uptake in terms of moles  $\text{CO}_2$  per mole of *total* AHA, both complexed and uncomplexed.

## 2.1 Physical absorption

Since we are interested here only in relatively low pressures, we will use a Henry's Law approach to model the physical solubility of  $\text{CO}_2$ . Kumelan et al.<sup>81</sup> have observed that for physical absorption of  $\text{CO}_2$  in ILs, specifically 1-hexyl-3-methylimidazolium bis(trifluoromethylsulfonyl)imide ([hmim][Tf<sub>2</sub>N]) and 1-butyl-3-methylimidazolium hexafluorophosphate ([bmim][PF<sub>6</sub>]), the relationship between the equilibrium  $\text{CO}_2$  pressure in the vapor phase and its molality in the liquid phase is remarkably linear, even up to pressures exceeding 90 bar. Carvalho and Coutinho<sup>82</sup> have even suggested that this pressure-molality line should be the same for any IL, though Gurkan and Brennecke<sup>83</sup> and Ramdin et al.<sup>52</sup> point out that this is actually a gross oversimplification. Ramdin et al.<sup>52</sup> also plot equilibrium  $\text{CO}_2$  pressure vs. molarity in several ILs and note a linear relationship up to about 60 bar, but this appears to be based on an incorrect computation of molarity, based on volume of solvent not volume of solution. While the volume expansion of an IL with addition of  $\text{CO}_2$  is not large, it is also not necessarily negligible (about 10-20% for  $\text{CO}_2$  mole fraction of 0.5).<sup>84</sup>

Since our mole ratio scale (moles  $\text{CO}_2$ /mole AHA) for physical  $\text{CO}_2$  uptake differs from molality only by a constant factor of the AHA molecular weight, we will model the equilibrium  $\text{CO}_2$  uptake by physical absorption using the linear relationship

$$X_{\text{phys}}^*(P_{\text{CO}_2}, T) = P_{\text{CO}_2} / H(T), \quad (4)$$

which is Henry's Law with a mole ratio composition scale. Here and below we use an asterisk to denote an equilibrium uptake value (mole ratio or mole fraction). To emphasize that this choice of a mole ratio composition scale is preferable to the more traditional mole fraction scale, we have plotted equilibrium  $\text{CO}_2$  uptake vs.  $\text{CO}_2$  pressure data<sup>85-87</sup> for three different physically absorbing ILs using both the mole ratio and mole fraction composition scales. These plots are shown in Figures 1-3, and show clearly that the mole ratio scale provides linearity over a much larger pressure range. Also, since the  $\text{CO}_2$  mole ratio  $X$  is related to the  $\text{CO}_2$  mole fraction  $x$  by  $X = x/(1-x)$ , it follows that  $X \rightarrow x$  in the low pressure limit ( $P_{\text{CO}_2} \rightarrow 0$  and  $x \rightarrow 0$ ). Thus,

the Henry's Law constant on the mole ratio scale and the Henry's Law constant on the mole fraction scale are the same:

$$H(T) = \lim_{P_{\text{CO}_2} \rightarrow 0} P_{\text{CO}_2} / X^* = \lim_{P_{\text{CO}_2} \rightarrow 0} P_{\text{CO}_2} / x^*. \quad (5)$$

The Henry's Law constant is related to the standard molar enthalpy  $\Delta h_{\text{phys}}^0$  and standard molar entropy  $\Delta s_{\text{phys}}^0$  of physical absorption by

$$H(T) = \exp\left(\frac{\Delta h_{\text{phys}}^0}{RT}\right) \exp\left(\frac{-\Delta s_{\text{phys}}^0}{R}\right). \quad (6)$$

We will assume that the enthalpy and entropy of physical absorption are constant (temperature independent) and equal to their standard values; that is,  $\Delta h_{\text{phys}} = \Delta h_{\text{phys}}^0$  and  $\Delta s_{\text{phys}} = \Delta s_{\text{phys}}^0$ . We also assume that the Henry's Law constant for physical absorption of  $\text{CO}_2$  in AHA is the same as for physical absorption of  $\text{CO}_2$  in AHA- $\text{CO}_2$ .

## 2.2 Chemical and physical absorption—1:1 chemical uptake

For 1:1 chemical absorption, based on the reaction given in Eq. (1), the reaction equilibrium can be expressed as  $K(T) = x_{\text{AHAX}} / (x_{\text{AHA0}} P_{\text{CO}_2})$ , where  $x_{\text{AHAX}}$  is the liquid-phase mole fraction of the AHA- $\text{CO}_2$  complex and  $x_{\text{AHA0}}$  is the liquid-phase mole fraction of uncomplexed AHA. This assumes an ideal vapor phase, and equality of the liquid-phase activity coefficients for AHA and AHA- $\text{CO}_2$  (this is consistent with the assumption that the physical solubility of  $\text{CO}_2$  is the same in both species and representable by a single Henry's Law constant). Assuming there are  $N$  total moles of AHA (complexed and uncomplexed), so that  $N = n_{\text{AHA0}} + n_{\text{AHAX}}$ , where  $n_{\text{AHAX}}$  and  $n_{\text{AHA0}}$  represent moles of complexed and uncomplexed AHA, respectively, in the liquid phase, then  $n_{\text{AHAX}} = K(T) P_{\text{CO}_2} (N - n_{\text{AHAX}})$ , which after rearrangement gives  $X_{\text{chem}}^* = n_{\text{AHAX}} / N = K(T) P_{\text{CO}_2} / (1 + K(T) P_{\text{CO}_2})$ . This is the chemical absorption analogue<sup>88</sup> of the Langmuir adsorption isotherm, and suggests an interpretation of the chemical absorption process as occurring at specific and independent absorption sites (in this case, one site per AHA anion) with  $X_{\text{chem}}^*$  corresponding to the fractional site coverage at

equilibrium. Since all sites may not be available, perhaps due to ion aggregation, we introduce an empirical factor  $X_{\text{chem}}^0(T) (\leq 1)$  corresponding to the maximum possible fractional site coverage, with  $X_{\text{chem}}^0(T) = C_1 - C_2(T - 273.15)$ . Thus, to model the equilibrium chemical uptake we use

$$X_{\text{chem}}^*(P_{\text{CO}_2}, T) = \frac{X_{\text{chem}}^0(T)K(T)P_{\text{CO}_2}}{1 + K(T)P_{\text{CO}_2}}. \quad (7)$$

The equilibrium constant is related to the standard molar enthalpy  $\Delta h_{\text{chem}}^0$  and standard molar entropy  $\Delta s_{\text{chem}}^0$  of chemical absorption by

$$K(T) = \exp\left(\frac{-\Delta h_{\text{chem}}^0}{RT}\right) \exp\left(\frac{\Delta s_{\text{chem}}^0}{R}\right). \quad (8)$$

We will assume that the enthalpy and entropy of chemical absorption are constant (temperature independent) and equal to their standard values; that is  $\Delta h_{\text{chem}} = \Delta h_{\text{chem}}^0$  and  $\Delta s_{\text{chem}} = \Delta s_{\text{chem}}^0$ .

Adding the physical and chemical contributions, the model for total  $\text{CO}_2$  uptake at equilibrium is then

$$X^*(P_{\text{CO}_2}, T) = \frac{P_{\text{CO}_2}}{H(T)} + \frac{X_{\text{chem}}^0(T)K(T)P_{\text{CO}_2}}{1 + K(T)P_{\text{CO}_2}}. \quad (9)$$

To demonstrate this model we will fit it to  $\text{CO}_2$  uptake data for three different AHAs: tetrabutylphosphonium 3-trifluoromethylpyrazolide ( $[\text{P}_{4444}][3\text{-CF}_3\text{pyra}]$ ), tetrabutylphosphonium 6-bromo-benzimidazolide ( $[\text{P}_{4444}][6\text{-BrBnim}]$ ), and trihexyl(tetradecyl)phosphonium 2-(cyano)pyrrolide ( $[\text{P}_{66614}][2\text{-CNpyr}]$ ). The equilibrium uptake data for these AHAs are shown in Figs. 4-6. For  $[\text{P}_{66614}][2\text{-CNpyr}]$ , the uptake data shown (Fig. 6) for pressures up to 1 bar are taken from Gurkan et al.<sup>46</sup> All other uptake data shown in Figs. 4-6 has been newly measured using gravimetric analysis, as described in detail by Bennett,<sup>89</sup> who also provides information on AHA synthesis and purity (98% for these three AHAs). The AHAs were dried in situ with a  $10^{-9}$  bar vacuum, so their water contents were negligible. Also shown in Figs. 4-6 are the model calculations, with the fit model parameters given in the captions. Values of  $\Delta h_{\text{chem}}$  have also been measured by calorimetry for some AHAs,<sup>90</sup> including  $[\text{P}_{66614}][2\text{-CNpyr}]$ . For this AHA, the

$\Delta h_{\text{chem}}$  from calorimetry is 45.2 kJ/mol (average of three runs with  $\pm 5\%$  uncertainty), in comparison to a value of 45.0 kJ/mol determined by fitting equilibrium uptake data to Eq. (9). The results of Figs. 4-6 demonstrate that the relatively simple  $\text{CO}_2$  uptake isotherm model of Eq. (9) can provide reasonable estimates of  $\text{CO}_2$  uptake. This isotherm model will be used in connection with the simple process model described in the next section.

### 2.3 Chemical and physical absorption—2:1 chemical uptake

We also consider the possibility of an IL absorbent (not necessarily an AHA) capable of 2:1 chemical uptake through an activated-site mechanism, as represented by



The IL has one active site for  $\text{CO}_2$  absorption, and reaction with  $\text{CO}_2$  at that site activates a second site on the IL- $\text{CO}_2$  complex, which can then absorb a second  $\text{CO}_2$  molecule. Proceeding as in Section 2.2, an isotherm model for the total chemical and physical  $\text{CO}_2$  uptake at equilibrium can be determined. This isotherm model is given by

$$X^*(P_{\text{CO}_2}, T) = \frac{P_{\text{CO}_2}}{H(T)} + \frac{X_{\text{chem}}^0(T) \left[ K_1(T) P_{\text{CO}_2} + 2K_1(T) K_2(T) P_{\text{CO}_2}^2 \right]}{1 + K_1(T) P_{\text{CO}_2} + K_1(T) K_2(T) P_{\text{CO}_2}^2}. \quad (12)$$

Here we again use an empirical factor  $X_{\text{chem}}^0(T) (\leq 1)$  corresponding to the maximum possible fractional site coverage, and the equilibrium constants  $K_1(T)$  and  $K_2(T)$ , for absorption at the first and second sites respectively, are related to the corresponding standard molar enthalpies and entropies by

$$K_1(T) = \exp\left(\frac{-\Delta h_{\text{chem},1}^0}{RT}\right) \exp\left(\frac{\Delta s_{\text{chem},1}^0}{R}\right) \quad (13)$$

and

$$K_2(T) = \exp\left(\frac{-\Delta h_{\text{chem},2}^0}{RT}\right) \exp\left(\frac{\Delta s_{\text{chem},2}^0}{R}\right). \quad (14)$$

One IL that we have identified as exhibiting this type of uptake behavior is trihexyl(tetradecyl)phosphonium 2-(1H-pyrrol-2-ylmethyl)pyrrolide ( $[P_{66614}][PMP]$ ), which was obtained in 95% purity. The equilibrium  $CO_2$  uptake data and model calculations for this IL are shown in Fig. 7, with the model parameters given in the captions. As explained in more detail by Bennett,<sup>89</sup> the experimental uptake values at the higher  $CO_2$  pressures are very likely to be somewhat lower than the actual uptake, because of the inability to do a proper buoyancy correction in the gravimetric analysis. Note the presence of an inflection point in both the model curve and experimental data (the model will exhibit an inflection point when  $K_1 < 2K_2$ ; see Supporting Information). The inflection point is characteristic of *cooperative binding*, a feature that may be exploited in designing absorption-desorption cycles. The presumed mechanism in the case of  $[P_{66614}][PMP]$  is that the absorption sites are at the nitrogen atoms in the PMP anion. In the uncomplexed IL, there is one protonated nitrogen (NH) and one unprotonated ( $N^-$ ). In the first absorption,  $CO_2$  absorbs at the  $N^-$  to give  $NCOO^-$ , which then deprotonates the other nitrogen, resulting in  $NCOOH$  and another active  $N^-$ , which can now absorb another  $CO_2$  molecule. Unfortunately, this IL is not a practical absorbent since it is highly viscous. Note that this IL is not an AHA (the anions in the IL and both of its complexed forms are protic).

### 3. A Simple Process Model

To address the simultaneous process and materials design problem posed in Section 1, we will use a simple process model of  $CO_2$  capture from post-combustion flue gas. This is an equilibrium-based material and energy balance model, comparable in complexity to the absorber-stripper model used by Oyarzún et al.<sup>77</sup> in their study of solvent design for physical absorption of  $CO_2$ . The model does not attempt to account for rate effects or viscous losses. The model is used to determine flowrates, heat duties, and process conditions that minimize a simple energy usage objective function. The sensitivity of this optimum with respect to various material properties and process parameters will then be studied.

A block diagram for the process model is shown in Figure 8. We will consider processing flue gas from both coal and natural gas fired power plants. The flue gas feed (stream 0) and  $CO_2$  product (stream 9) specifications are taken from a detailed DOE/NETL study<sup>50</sup> of

power plant economics with and without carbon capture (our reference cases are drawn from Revision 2a<sup>50</sup> of this study; the corresponding cases in Revision 3<sup>51</sup> are slightly different). Specifically, for the coal case, our reference inputs and outputs are streams 18 and 21 in Case 10, a subcritical pulverized coal (PC) power plant that has a net output of 550 MWe, and, for the natural gas case, streams 4 and 7 in Case 14, a natural gas combined cycle (NGCC) power plant that has a net output of 474 MWe. Detailed flue gas feed specifications for both cases are given in Table 1. The final CO<sub>2</sub> product is specified to be at a pressure of  $P_9 = 152.7$  bar, dehydrated to a dew point below  $-40$  °C. It is specified that 90% of the entering CO<sub>2</sub> is captured and leaves in the product stream.

The absorber is treated as isothermal at  $T_a$ , with heat removal rate  $Q_a$ , pressure  $P_a$ , and precooling of feed. The absorber inlet temperature  $T_1$  is assumed to be fixed by the available cooling water temperature  $T_{cw}$  and specified minimum approach temperature  $\Delta T_{appr}$  by  $T_1 = T_{cw} + \Delta T_{appr}$ . Since the flue gas feed is at  $P_0 = 1$  bar, a feed blower with pre-cooled feed is included to allow for the possibility of  $P_a > 1$  bar. In the feed pretreatment process, any condensed water will be removed. We will consider both the idealized case of infinite absorber stages and the case of a finite number of stages. Since the recovered CO<sub>2</sub> must eventually be compressed to high pressure for delivery, there may be some advantage to using a pump on the rich liquid stream 4 to achieve some of this pressure increase. Thus, the stripper pressure  $P_s$  may be greater than  $P_a$ , with the tradeoff that this either reduces the difference in uptake between the absorber and stripper or requires a higher stripper temperature to achieve the same difference in uptake. In this case, there will be a pressure reduction on the lean liquid recycle to the absorber, but no work credit will be taken. It is also possible for  $P_s$  to be less than  $P_a$  (pressure-swing process); in this case there is a pump for the lean liquid stream 7, and a pressure reduction in the rich liquid feed to the stripper, again with no energy credit taken. Note that pump work may be done on either stream 4 or stream 7, but not both. Heat integration is provided by using the solvent recycle from the stripper to preheat the stripper input. The stripper is treated as a single equilibrium stage,<sup>91,92</sup> with heat input rate  $Q_s$  and temperature  $T_s$ . Since the vapor pressure of the AHA is exceedingly low, we assume that there are no solvent losses; that is, the total flowrate of AHA (complexed and uncomplexed) circulating in streams 2, 4, 5 and 7 is constant.

The components present in the feed are CO<sub>2</sub>, H<sub>2</sub>O, N<sub>2</sub>, O<sub>2</sub> and Ar. There is no chemical absorption and no appreciable physical absorption of N<sub>2</sub>, O<sub>2</sub> and Ar into the AHA solvent,<sup>89</sup> so these components are treated as inert. We will also assume that there is no absorption of water by the AHA. However, this may not always be a good assumption. We will discuss the potential impact of water absorption in Section 4.4.

We will focus here on modeling the CO<sub>2</sub> capture section of the process with stream 1 as input and streams 3 and 6 as outputs (the compression and pretreatment sections will be dealt with separately). The molar flowrate of component  $j$  in stream  $i$  is denoted by  $F_{i,j}$  and the total molar flowrate of stream  $i$  by  $F_i$ . Since water will likely be removed by condensation during the feed pretreatment process, we adjust the composition of the absorber feed (stream 1) to account for this. The mole fraction of water after pretreatment will be given by

$$y_{1,\text{H}_2\text{O}} = \min\{y_{0,\text{H}_2\text{O}}, P_{\text{H}_2\text{O}}^{\text{sat}}(T_1)/P_1\}, \quad (15)$$

where  $P_{\text{H}_2\text{O}}^{\text{sat}}(T)$  is the vapor pressure of water as a function of temperature. For this we use the dimensional formula (Antoine equation)<sup>93</sup>

$$\log_{10} P_{\text{H}_2\text{O}}^{\text{sat}}[\text{bar}] = 6.20963 - \frac{2354.731}{7.559 + T[\text{K}]}. \quad (16)$$

If condensation of water does occur ( $y_{1,\text{H}_2\text{O}} < y_{0,\text{H}_2\text{O}}$ ), then the adjusted flowrate is

$$F_1 = F_0 \left( \frac{1 - y_{0,\text{H}_2\text{O}}}{1 - y_{1,\text{H}_2\text{O}}} \right) \quad (17)$$

and the adjusted mole fractions are

$$y_{1,j} = y_{0,j} \left( \frac{1 - y_{1,\text{H}_2\text{O}}}{1 - y_{0,\text{H}_2\text{O}}} \right), \quad j = \text{CO}_2, \text{N}_2, \text{O}_2, \text{Ar}. \quad (18)$$

Before writing the material and energy balances for this system, we first will develop expressions for the enthalpy flow rates, assuming AHAs with 1:1 chemical uptake. We will assume negligible pressure drops in the absorber, stripper and heat exchanger, and treat vapor streams as ideal. Streams 1 and 3 are vapor mixtures of CO<sub>2</sub>, H<sub>2</sub>O, O<sub>2</sub>, N<sub>2</sub> and Ar. Their enthalpy flow rates are

$$H_i = \sum_j F_{i,j} \int_{T_{\text{ref}}}^{T_i} C_{p,j}(T) dT, \quad j = \text{CO}_2, \text{H}_2\text{O}, \text{N}_2, \text{O}_2, \text{Ar}, \quad i = 1,3, \quad (19)$$

where  $C_{p,j}(T)$  is the molar heat capacity of species  $j$ , and  $T_{\text{ref}}$  is an arbitrary reference temperature. Similarly, for the vapor stream 6, which is assumed to be pure  $\text{CO}_2$ ,

$$H_6 = \sum_j F_{6,j} \int_{T_{\text{ref}}}^{T_6} C_{p,j}(T) dT, \quad j = \text{CO}_2. \quad (20)$$

The heat capacities are calculated from the Shomate equation, with parameters from the NIST Chemistry WebBook.<sup>93</sup>

Streams 2, 4 and 7 are liquid mixtures of complexed and uncomplexed AHA, plus physically absorbed  $\text{CO}_2$ . Their enthalpy flowrates are

$$H_i = \sum_j F_{i,j} \int_{T_{\text{ref}}}^{T_i} C_{p,j}(T) dT + q_i(P_i - P_{\text{ref}}) + F_{i,\text{AHAX}} \Delta h_{\text{chem}} + F_{i,\text{CO}_2} \Delta h_{\text{phys}}, \quad (21)$$

$$j = \text{AHA0}, \text{AHAX}, \text{CO}_2, \quad i = 2,4,7.$$

Here  $\Delta h_{\text{chem}}$  and  $\Delta h_{\text{phys}}$  are the molar heats of chemical and physical absorption, respectively, of  $\text{CO}_2$ ,  $q_i$  is the volumetric flow rate of stream  $i$ , and  $P_{\text{ref}}$  is an arbitrary reference pressure. For  $\Delta h_{\text{chem}}$  and  $\Delta h_{\text{phys}}$ , the standard values are used, as discussed in Section 2. We will assume that the heat capacity of the complexed AHA is equal to the heat capacity of the uncomplexed AHA plus the heat capacity of  $\text{CO}_2$ ; that is,  $C_{p,\text{AHAX}}(T) = C_{p,\text{AHA0}}(T) + C_{p,\text{CO}_2}(T)$  (this is consistent with the earlier assumption that the enthalpy and entropy of chemical absorption are temperature independent). With this assumption, it will be convenient to rewrite Eq. (21) as

$$H_i = \left( F_{i,\text{AHA0}} + F_{i,\text{AHAX}} \right) \int_{T_{\text{ref}}}^{T_i} C_{p,\text{AHA0}}(T) dT + q_i(P_i - P_{\text{ref}}) + F_{i,\text{AHAX}} \Delta h_{\text{chem}} \quad (22)$$

$$+ F_{i,\text{CO}_2} \Delta h_{\text{phys}} + (F_{i,\text{CO}_2} + F_{i,\text{AHAX}}) \int_{T_{\text{ref}}}^{T_i} C_{p,\text{CO}_2}(T) dT, \quad i = 2,4,7.$$

For the heat capacity of the uncomplexed AHA, we will assume a linear temperature dependence,  $C_{p,\text{AHA0}}(T) = A + BT$ , as suggested by Crosthwaite et al.,<sup>94</sup> with the parameters  $A = 630 \text{ J}/(\text{mol K})$  and  $B = 1.89 \text{ J}/(\text{mol K}^2)$  as reported by Seo et al.<sup>63</sup> for  $[\text{P}_{66614}][2\text{-CNpyr}]$ . Since

stream 4 will have a high CO<sub>2</sub> uptake (saturated with CO<sub>2</sub> in the infinite-stage case), we should anticipate that stream 5 will be a two-phase (vapor plus liquid) stream due to heating in the heat exchanger. However, in the development that follows, we will not need an explicit expression for  $H_5$ .

We will do material and energy balances on a basis of one mole of total AHA (complexed and uncomplexed) in circulation. On this basis, the stream enthalpies are  $\tilde{H}_i = H_i / F_{\text{AHA}}$ ,  $i=1,2,\dots,7$ , where  $F_{\text{AHA}} = F_{i,\text{AHA}0} + F_{i,\text{AHAX}}$ ,  $i=2,4,5,7$ , has the same value in all streams in the AHA circulation loop. This choice of basis allows the balance equations to be written in terms of the CO<sub>2</sub> uptake (moles absorbed per mole total AHA). Per mole of total AHA, the stream enthalpies are

$$\tilde{H}_i = \sum_j \tilde{F}_{i,j} \int_{T_{\text{ref}}}^{T_i} C_{p,j}(T) dT, \quad j = \text{CO}_2, \text{H}_2\text{O}, \text{N}_2, \text{O}_2, \text{Ar}, \quad i=1,3 \quad (23)$$

$$\tilde{H}_6 = \sum_j \tilde{F}_{6,j} \int_{T_{\text{ref}}}^{T_6} C_{p,j}(T) dT, \quad j = \text{CO}_2 \quad (24)$$

$$\begin{aligned} \tilde{H}_i = & \int_{T_{\text{ref}}}^{T_i} C_{p,\text{AHA}0}(T) dT + X_i \int_{T_{\text{ref}}}^{T_i} C_{p,\text{CO}_2}(T) dT + X_{i,\text{chem}} \Delta h_{\text{chem}} + X_{i,\text{phys}} \Delta h_{\text{phys}} \\ & + \tilde{q}_i (P_i - P_{\text{ref}}), \quad i = 2,4,7 \end{aligned} \quad (25)$$

Here, for stream  $i$ , the notation  $X_i = X_{i,\text{chem}} + X_{i,\text{phys}}$  refers to CO<sub>2</sub> uptake, as in Section 2,  $\tilde{q}_i = q_i / F_{\text{AHA}}$  is the volumetric flow rate per mole of AHA in circulation, and  $\tilde{F}_{i,j} = F_{i,j} / F_{\text{AHA}}$  is the vapor flow of component  $j$  per mole of AHA in circulation.

The overall CO<sub>2</sub> balance, together with the specification of 90% capture, gives  $\tilde{F}_{3,\text{CO}_2} = 0.1\tilde{F}_{1,\text{CO}_2}$  and  $\tilde{F}_{6,\text{CO}_2} = 0.9\tilde{F}_{1,\text{CO}_2}$ . Balances on heat exchanger and stripper give  $X_2 = X_7 = X_4 - \tilde{F}_{6,\text{CO}_2} = X_4 - 0.9\tilde{F}_{1,\text{CO}_2}$  or  $0.9\tilde{F}_{1,\text{CO}_2} = X_4 - X_7$ . The stripper is treated as a single equilibrium stage,<sup>91,92</sup> so

$$X_7 = X_2 = X^*(P_{s,\text{CO}_2}, T_s) = X^*(P_s, T_s). \quad (26)$$

We specify that the recycled AHA must be sufficiently lean to provide a minimum uptake driving force of at least 0.01 at the top of the absorption column. That is,  $X^*(P_{3,\text{CO}_2}, T_a) - X_2 \geq 0.01$ . For the absorber uptake, we use

$$X_4 = X^*(P_{1,\text{CO}_2}, T_a) - \Delta X_{\text{appr}} = X^*(P_a y_{1,\text{CO}_2}, T_a) - \Delta X_{\text{appr}}, \quad (27)$$

where  $\Delta X_{\text{appr}} (\geq 0)$  is a specified approach to the saturation uptake  $X^*(P_{1,\text{CO}_2}, T_a)$ . For an infinite stage absorber,  $\Delta X_{\text{appr}} = 0$ , and for a single stage absorber,  $\Delta X_{\text{appr}} = X^*(P_{1,\text{CO}_2}, T_a) - X^*(P_{3,\text{CO}_2}, T_a)$ . Thus, for specified absorber and stripper conditions, the required AHA flow rate  $F_{\text{AHA}}$  can be calculated from

$$F_{\text{AHA}} = \frac{0.9F_{1,\text{CO}_2}}{X_4 - X_7} = \frac{0.9F_{1,\text{CO}_2}}{(X^*(P_a y_{1,\text{CO}_2}, T_a) - \Delta X_{\text{appr}}) - (X^*(P_s, T_s))}. \quad (28)$$

The energy balance equations are, for the absorber,

$$\tilde{H}_1 + \tilde{H}_2 - \tilde{H}_3 - \tilde{H}_4 - \tilde{Q}_a = 0, \quad (29)$$

for the stripper,

$$\tilde{H}_5 - \tilde{H}_6 - \tilde{H}_7 + \tilde{Q}_s = 0, \quad (30)$$

and for the pump plus heat exchanger,

$$\tilde{H}_4 + \tilde{H}_7 - \tilde{H}_5 - \tilde{H}_2 + \tilde{W}_p = 0, \quad (31)$$

where the heat duties  $\tilde{Q}_a = Q_a / F_{\text{AHA}}$  and  $\tilde{Q}_s = Q_s / F_{\text{AHA}}$ , and pump work  $\tilde{W}_p = W_p / F_{\text{AHA}}$  are per mole of total AHA in circulation. These balances involve the seven stream temperatures, of which one is fixed by  $T_1 = T_{\text{cw}} + \Delta T_{\text{appr}}$ , and four are determined by the absorber and stripper operating conditions,  $T_3 = T_4 = T_a$ , and  $T_6 = T_7 = T_s$ . The remaining temperatures,  $T_2$  and  $T_5$ , must satisfy

$$\left. \begin{array}{l} (T_2 - T_a) - \Delta T_{\text{appr}}, \quad \text{if } \tilde{C}_{a \rightarrow 5} > \tilde{C}_{s \rightarrow 2} \\ (T_s - T_5) - \Delta T_{\text{appr}}, \quad \text{if } \tilde{C}_{a \rightarrow 5} \leq \tilde{C}_{s \rightarrow 2} \end{array} \right\} = 0, \quad (32)$$

where  $\tilde{C}_{a \rightarrow 5} = (\tilde{H}_5 - \tilde{H}_a) / (T_5 - T_a)$  and  $\tilde{C}_{s \rightarrow 2} = (\tilde{H}_2 - \tilde{H}_s) / (T_2 - T_s)$  are the effective heat capacity flows per mole of total AHA in circulation for the streams exchanging heat. While the hot (s  $\rightarrow$  2) stream will have somewhat higher molar heat capacity than the cold (a  $\rightarrow$  5) stream,

due to its higher temperature and reduced CO<sub>2</sub> content, the hot stream will also have a significantly lower molar flowrate, due to the removal of CO<sub>2</sub> in the stripper. Thus, in our experience, for process conditions of interest, it is always true that the heat capacity flow of the hot stream is less than that of the cold stream, i.e.  $\tilde{C}_{a \rightarrow 5} > \tilde{C}_{s \rightarrow 2}$ . This means that Eq. (32) can be replaced by  $T_2 = T_a + \Delta T_{\text{appr}}$ , relating  $T_2$  directly to the absorber operating condition, and that it is not necessary to determine  $T_5$ . Thus, we can eliminate  $T_5$  and one of the energy balances by combining Eqs. (30) and (31) to obtain

$$\tilde{H}_4 - \tilde{H}_6 - \tilde{H}_2 + \tilde{Q}_s + \tilde{W}_p = 0, \quad (33)$$

a balance on the subsystem of pump, heat exchanger and stripper.

To optimize the system we will use a simple parasitic energy objective function, expressed in terms of total electrical power used,

$$E = \left( \alpha \tilde{Q}_s + \frac{\tilde{W}_p}{\eta_p} \right) F_{\text{AHA}} + W_b + W_c, \quad (34)$$

where  $\eta_p = 0.75$  is the pump efficiency and  $\alpha$  is the ‘‘power equivalence factor’’ This factor relates the heat content of steam withdrawn from the power plant steam cycle to the corresponding loss of power output. That is, for withdrawal of steam heat content  $\tilde{Q}_s$ , the loss of power plant output is  $\alpha \tilde{Q}_s$ . Thus,  $\alpha$  can be regarded as conversion factor from thermal to electrical energy.

From Eq. (33) together with Eqs. (24) and (25), we can determine  $\tilde{W}_p$  and  $\tilde{Q}_s$ . For the pump work,  $\tilde{W}_p = v_{\text{AHA}}(P_2 - P_4)$  if  $P_s > P_a$  or  $\tilde{W}_p = v_{\text{AHA}}(P_2 - P_7)$  if  $P_s < P_a$ ; thus

$$\tilde{W}_p = v_{\text{AHA}} |P_s - P_a|, \quad (35)$$

where we have assumed that the volume change of absorption is negligible, so that  $\tilde{q}_2 = \tilde{q}_4 = \tilde{q}_7 = v_{\text{AHA}}$ , the molar volume of the AHA. For the stripper heat,

$$\begin{aligned} \tilde{Q}_s = & (X_{7,\text{chem}} - X_{4,\text{chem}})\Delta h_{\text{chem}} + (X_{7,\text{phys}} - X_{4,\text{phys}})\Delta h_{\text{phys}} \\ & + \int_{T_a}^{T_2} C_{p,\text{AHA0}}(T)dT + X_4 \int_{T_a}^{T_s} C_{p,\text{CO}_2}(T)dT - X_7 \int_{T_2}^{T_s} C_{p,\text{CO}_2}(T)dT, \end{aligned} \quad (36)$$

where we have used the relations  $X_2 = X_7$ ,  $T_6 = T_s$  and  $T_4 = T_a$ . Here the first two terms represent the energy needed to desorb the  $\text{CO}_2$ , the third term represents the net sensible heating of the AHA, and the last two terms represent the net sensible heating of the  $\text{CO}_2$ , in either absorbed or desorbed form.  $X_4$  and  $X_7$  are given in terms of the absorber and stripper conditions by Eqs. (26) and (27), and there are similar relations for the separate chemical and physical uptakes

$$X_{7,\text{chem}} = X_{\text{chem}}^*(P_s, T_s). \quad (37)$$

$$X_{7,\text{phys}} = X_{\text{phys}}^*(P_s, T_s). \quad (38)$$

$$X_{4,\text{chem}} = X_{\text{chem}}^*(P_a y_{1,\text{CO}_2}, T_a) \left[ 1 - \frac{\Delta X_{\text{appr}}}{X^*(P_a y_{1,\text{CO}_2}, T_a)} \right], \quad (39)$$

$$X_{4,\text{phys}} = X_{\text{phys}}^*(P_a y_{1,\text{CO}_2}, T_a) \left[ 1 - \frac{\Delta X_{\text{appr}}}{X^*(P_a y_{1,\text{CO}_2}, T_a)} \right], \quad (40)$$

Here the deviation from saturation in the absorber outlet  $\Delta X_{\text{appr}}$  has been assigned to the chemical and physical components according to their relative proportion. Finally, noting that  $T_2 = T_a + \Delta T_{\text{appr}}$ , it can be seen that both  $\tilde{W}_p$  and  $\tilde{Q}_s$  are functions only of the absorber and stripper operating conditions ( $T_a, P_a, T_s, P_s$ ).

For the feed blower, we will assume isentropic compression with a specified efficiency  $\eta_b = 0.75$ ; thus the work requirement is

$$W_b = \frac{F_b R T_{\text{in}} k}{\eta_b (k-1)} \left[ \left( \frac{P_a}{P_0} \right)^{\frac{k-1}{k}} - 1 \right]. \quad (41)$$

Here the blower inlet temperature  $T_{\text{in}}$  is assumed given by  $T_{\text{in}} = T_{\text{cw}} + \Delta T_{\text{appr}}$ , and the heat capacity ratio  $k = C_v / C_p$  is taken to be  $k = 1.37$  for the PC case and  $k = 1.39$  for the NGCC case. These values are based on the specified flue gas composition and averaged over the anticipated temperature range. The blower flowrate  $F_b$  is determined by evaluating Eqs. (15)-(17) for the case  $T_1 = T_{\text{in}}$  and  $P_1 = P_0 = 1$  bar.

To calculate the compressor work, we will use a method based on the approach used by McCollum and Ogden<sup>95</sup> in the context of techno-economic analysis of  $\text{CO}_2$  compression. It is

assumed that there are six intercooled stages. The first five take the feed up to a cut-off of  $P_c = 73.8$  bar (critical pressure of  $\text{CO}_2$ ) and are modeled as compressors. The sixth stage, which deals with liquid or supercritical  $\text{CO}_2$  is modeled as a pump. For the five compressor stages, it is assumed that the compression ratio is the same in each stage (a common heuristic). This gives a compression ratio of  $r_c = (P_c / P_s)^{1/5}$ . The compression work is then calculated by assuming isentropic compression with an isentropic efficiency of  $\eta_c$ . Values for the heat capacity ratio  $k$  and compressibility factor  $Z$  are also required. McCollum and Ogden<sup>95</sup> do a stage-by-stage calculation using  $k$  and  $Z$  values that are averages over the pressure range of each stage, assuming a feed of 1 bar. To simplify, we will take the average of these five values and then use these average values of  $k$  and  $Z$  for all compression stages. The total compression work, per mole of  $\text{CO}_2$  removed, is then

$$\frac{W_c}{F_{6,\text{CO}_2}} = \frac{W_c}{0.9F_{1,\text{CO}_2}} = \frac{5ZRT_8k}{\eta_c(k-1)} \left[ r_c^{\left(\frac{k-1}{k}\right)} - 1 \right] + \frac{M(P_9 - P_c)}{\rho\eta_p}. \quad (42)$$

Here  $T_8$  is the inlet temperature, taken to be the same for each intercooled compression stage, and assumed to be  $T_8 = T_{\text{cw}} + \Delta T_{\text{appr}}$ ,  $M = 44.01$  g/mol is the molecular weight of  $\text{CO}_2$ ,  $P_9$  is specified to be 152.7 bar, and  $\rho$  is the density of  $\text{CO}_2$ . Following McCollum and Ogden,<sup>95</sup> we use  $\eta_c = 0.75$ ,  $\eta_p = 0.75$  and  $\rho = 630$  kg/m<sup>3</sup>. The averaged values of  $k$  and  $Z$  used are  $k = 1.391$  and  $Z = 0.946$ .

For the power equivalence factor  $\alpha$ , there have been several different values and methods used, as noted by Peeters et al.<sup>96</sup> and critiqued by Lucquiaud and Gibbins.<sup>97</sup> Our approach is based on the simple method given by Oyenekan and Rochelle.<sup>49,98</sup> In this approach we start with the theoretical maximum (Carnot) heat to work efficiency of  $1 - (T_{\text{cold}} / T_{\text{hot}})$  and then multiply by a ‘‘Carnot factor’’ or ‘‘integration factor’’  $\beta$  that reflects the deviation of the actual work lost to this theoretical maximum. The value of  $\beta$  can be thought of as an indication of the efficiency with which the carbon capture unit has been integrated with the power plant (smaller  $\beta$  reflects better integration). If  $T_{\text{hot}} = T_{\text{steam}} = T_s + \Delta T_{\text{appr}}$  and  $T_{\text{cold}} = T_{\text{cw}} + \Delta T_{\text{appr}}$ , then

$$\alpha = \beta \left[ 1 - \frac{T_{\text{cw}} + \Delta T_{\text{appr}}}{T_s + \Delta T_{\text{appr}}} \right]. \quad (43)$$

Following Oyenekan and Rochelle,<sup>49,98</sup> we will use  $\beta = 0.75$ . While this method does not account for all of the complexities of the situation,<sup>97</sup> its use avoids the need for a full power plant model and makes the important connection between stripper temperature and loss of power output. However, it should be recognized that there is considerable uncertainty in the value of  $\beta$ . For typical  $T_{\text{hot}}$  and  $T_{\text{cold}}$  in this context, the range of  $\alpha$  values (0.097 to 0.329) reported by Peeters et al.<sup>96</sup> corresponds to a range of  $\beta$  values of about 0.3 to 1.

The objective  $E$  does not account for the energy needed for the cooling towers used to generate cooling water. Also, since the model used is equilibrium based, viscous and dynamic effects are not accounted for. The model developed in this section for the case of an AHA with 1:1 CO<sub>2</sub> uptake (Section 2.2) can easily be modified to also deal with the case of an IL absorbent with 2:1 uptake (Section 2.3).

## 4. Results and Discussion

The energy objective  $E$  given in Eq. (34) is a function of the decision variables  $T_a$ ,  $P_a$ ,  $T_s$ , and  $P_s$ . The objective function also depends on the values of various other material and process parameters, as well as the integration factor  $\beta$ ; given values of these “sensitivity parameters”,  $E$  can be optimized with respect to  $T_a$ ,  $P_a$ ,  $T_s$ , and  $P_s$ , and an optimal value  $E^*$  determined. The optimization was done using a differential evolution<sup>99</sup> method that we developed and tuned specifically for this problem. In this Section, we will explore the variation of  $E^*$  with changes in the sensitivity parameters, and use the results of these studies to suggest appropriate material and process parameter values. For all such sensitivity studies, some AHA material parameters are held fixed, as indicated in Table 2. The fixed values used correspond to the AHA [P<sub>66614</sub>][2-CNpyr]. Table 2 also lists the sensitivity parameters considered, along with their base values and the range studied. The base values are the default values used, unless otherwise specified. The range constraints on the decision variables are also given in Table 2.

### 4.1 One-site chemical absorption—PC flue gas

We first consider flue gas from a pulverized coal power plant, as specified in Table 1, and use one-site chemical absorption. As a first sensitivity study we consider the variation in the optimal parasitic energy  $E^*$  with the chemical absorption enthalpy,  $\Delta h_{\text{chem}}$ , and entropy,

$\Delta s_{\text{chem}}$ , with other sensitivity parameters held at their base values (Table 2). The results are shown in Fig. 9, which plots contours of constant  $E^*$  (in units of megawatts electrical, MWe) vs.  $\Delta h_{\text{chem}}$  and  $\Delta s_{\text{chem}}$ . Note that each point on this plot represents an optimization problem in which  $E$  was optimized with respect to the absorber and stripper conditions,  $T_a$ ,  $P_a$ ,  $T_s$ , and  $P_s$ , to determine  $E^*$ . The plot shows a clear “valley” of low  $E^*$  values, from about  $\Delta h_{\text{chem}} = -46$  kJ/mol at  $\Delta s_{\text{chem}} = -120$  J/(mol K) and sloping slightly down (in  $E^*$  value) to about  $\Delta h_{\text{chem}} = -49$  kJ/mol at  $\Delta s_{\text{chem}} = -130$  J/(mol K), and  $\Delta h_{\text{chem}} = -52$  kJ/mol at  $\Delta s_{\text{chem}} = -140$  J/(mol K). The slope of the  $E^*$  contours indicates that  $E^*$  is about three times more sensitive to changes in  $\Delta h_{\text{chem}}$  than to changes in  $\Delta s_{\text{chem}}$ . The spacing of the contours shows that  $E^*$  values increase quickly as  $\Delta h_{\text{chem}}$  becomes less negative to the right of the valley, but increase slowly as  $\Delta h_{\text{chem}}$  becomes more negative to the left of the valley. The optimal values of the absorber and stripper conditions are shown in Fig. 10 for the case of  $\Delta s_{\text{chem}} = -130$  J/(mol K). This shows that the absorber temperature and stripper pressure are optimal at their lower bounds (Table 2) over the entire range of  $\Delta h_{\text{chem}}$  considered. The absorber pressure is optimal at its lower bound of 1 bar, except when the chemical absorption is not sufficiently strong (weaker than about  $-44$  kJ/mol); in this case, a higher pressure is needed to compensate for the weaker chemical binding. The optimized stripper temperature is a key quantity, as it achieves a minimum value very close to the optimal  $\Delta h_{\text{chem}}$  of about  $-49$  kJ/mol. If chemical binding is stronger than this, the optimized stripper temperature increases to compensate, until its upper limit of 473.15 K is reached. If it is weaker, the optimized stripper temperature increases to try to maintain a high cyclic capacity (the uptake difference  $X_4 - X_7$ ). With further decrease in chemical binding strength, an increase in the absorber pressure is preferred to further increase in the stripper temperature. Fig. 11 shows the variation in the optimized cyclic capacity with chemical binding strength for the case of  $\Delta s_{\text{chem}} = -130$  J/(mol K). It is noteworthy that the optimal binding energy of about  $-49$  kJ/mol does not correspond to the maximum cyclic capacity, which occurs at about  $-60$  kJ/mol. The higher optimized cyclic capacity at about  $-60$

kJ/mol occurs due to a significantly higher (by about 60 K) optimized stripper temperature, a temperature at which the power equivalence factor is higher and which requires additional sensible heating. The variation in the different components of the total optimized parasitic energy with chemical absorption enthalpy is shown in Fig. 12.

We now consider the sensitivity of the optimal parasitic energy  $E^*$  to other process and material properties. Figs. 13 and 14 show the sensitivity with respect to the cooling water temperature  $T_{\text{cw}}$  and the minimum approach temperature  $\Delta T_{\text{appr}}$ . While these parameters affect multiple aspects of the process, together they directly affect the minimum possible absorber temperature,  $T_{\text{cw}} + \Delta T_{\text{appr}}$ . Clearly, use of a lower absorber temperature improves performance and allows for a weaker optimal binding energy.  $\Delta T_{\text{appr}}$  also directly affects the performance of the heat exchanger providing heat integration between the rich and lean solvent streams. A higher  $\Delta T_{\text{appr}}$  will result in less preheating of the rich stream and thus a higher sensible heat requirement from external sources. This accounts for the higher sensitivity of  $E^*$  to  $\Delta T_{\text{appr}}$  than  $T_{\text{cw}}$  at the stronger binding energies that require a high stripper temperature. Fig. 15 shows the sensitivity with respect to the base AHA heat capacity parameter  $A$ ; a change in  $A$  (at constant temperature) results in an equal change in the AHA heat capacity value  $C_{\text{p,AHA0}}$ . A lower AHA heat capacity reduces the parasitic energy, due to its impact on the sensible heating required. Since the heat capacity of an IL is roughly proportional to its molecular weight,<sup>94</sup> this also implies that a lower molecular weight AHA is preferable. Sensitivity with respect to the process integration factor  $\beta$  is shown in Fig. 16. Since the value of  $\beta$  directly impacts the factor used to convert steam energy to electrical energy, it is not surprising that a lower  $\beta$  (better integration of carbon capture unit with power plant) reduces the parasitic energy. It is interesting, however, that the  $\beta$  value does not impact the location of the optimal binding energy.

The results presented so far have been for the case of an ideal, infinite-stage absorption process. We now consider the effect of actual absorption column performance. One way to specify absorber performance is to use  $\Delta X_{\text{appr}}$ , the approach to saturation of the rich CO<sub>2</sub>-rich AHA stream leaving the absorber (see Eq. (27)). Fig. 17 shows the sensitivity of the optimal parasitic energy  $E^*$  to changes in  $\Delta X_{\text{appr}}$ . It is interesting that even for a  $\Delta X_{\text{appr}}$  as large as 0.2

moles CO<sub>2</sub> per mole AHA (complexed and uncomplexed), the optimal binding energy increases only by about 1 kJ/mol. Another way to specify absorber performance is by the number of ideal stages ( $N_s$ ) it represents. When a value of  $N_s$  is specified, it must be converted into a corresponding value of  $\Delta X_{\text{appr}}$  in order to use the computational procedure outlined above. This is done iteratively, and since the result depends on the values of the decision variables ( $T_s$ ,  $T_a$ ,  $P_s$  and  $P_a$ ), must be embedded into the overall optimization procedure. Sensitivity to  $N_s$  is shown in Fig. 18. Also, the optimal absorber operating diagrams are shown in Figs. 19-21 for some selected cases with chemical absorption enthalpy from  $-45$  to  $-55$  kJ/mol. These diagrams also demonstrate the relationship between  $\Delta X_{\text{appr}}$  and  $N_s$ . The optimal parasitic energy curves are all rather flat near their minimum values, which occur, for two or more ideal stages, within the relatively narrow binding energy range of about  $-49$  kJ/mol (infinite stages) to  $-52$  kJ/mol (two ideal stages). Especially towards the lower end of this range, there appears to be little incentive to use more than two or three ideal stages. This can be understood by comparing the operating diagrams in Figs. 19-21. As the binding energy becomes stronger, the equilibrium curve becomes increasingly flat in the high uptake region, causing additional stages to result in little performance improvement. This is particularly evident in Fig. 21, where even two ideal stages closely approaches the infinite-stage performance ( $\Delta X_{\text{appr}} = 0$ ). For the case of two ideal absorber stages ( $N_s = 2$ ), with best-case values of other process parameters ( $T_{\text{cw}} = 293.15$  K,  $\Delta T_{\text{appr}} = 5$  K), the sensitivity of  $E^*$  with respect to  $\Delta h_{\text{chem}}$  is shown in Fig. 22. This indicates an optimal  $E^*$  of 107.2 MWe at about  $-49$  kJ/mol. This differs from standard carbon capture technology largely in the heat requirement  $Q_s$ , which is 271 MWth (megawatts thermal) for the case considered here and 586 MWth for Case 10 in the DOE/NETL study,<sup>50</sup> which uses the Econamine FG Plus<sup>SM</sup> process. On a per metric ton of CO<sub>2</sub> captured basis, these heat requirements become 1.64 GJ/t for the case considered here and 3.54 GJ/t for DOE/NETL Case 10.

The results presented above suggest that for  $-140 \leq \Delta s_{\text{chem}} \leq -120$  J/(mol K), there is a range of optimal chemical absorption strength of about  $-54$  to  $-48$  kJ/mol, and that if this target cannot be met, it is preferable to miss on the too strong side. This indicates that the AHAs whose uptakes are shown in Figs. 4-6, which have chemical absorption enthalpies in the range of

about  $-43$  to  $-45$  kJ/mol, are slightly below the optimal range. This is consistent with the analysis of Zhai and Rubin,<sup>100</sup> who indicate that for  $[P_{66614}][2\text{-CNpyr}]$  (Fig. 6)  $\text{CO}_2$  capture is most cost effective at only 85% removal, rather than the target 90%. However, other AHAs have already been synthesized and characterized which do have  $\Delta h_{\text{chem}}$  values in the desired range,<sup>63</sup> and, with this target range now identified, other promising AHAs may be sought.

#### 4.2 One-site chemical absorption—NGCC flue gas

We now consider flue gas from a natural gas combined cycle power plant, as specified in Table 1, and again use one-site chemical absorption. Fig. 23 shows the variation in the optimal parasitic energy  $E^*$  with  $\Delta h_{\text{chem}}$  and  $\Delta s_{\text{chem}}$  for this case, with other sensitivity parameters held at their base values (Table 2). Comparing to Fig. 9, the analogous plot for PC flue gas, shows that the “valley” of low  $E^*$  values has shifted towards stronger chemical binding. While a shift in this direction is not surprising, given that the concentration of  $\text{CO}_2$  in NGCC flue gas is much lower than in PC flue gas, our analysis allows us to quantify the shift at about  $-4$  kJ/mol for the base parameter values used for Fig. 23. Fig. 24 shows the optimal values of the absorber and stripper conditions for the case of  $\Delta s_{\text{chem}} = -130$  J/(mol K). Compared to the PC flue gas case (Fig. 10), the primary difference is that a higher stripper temperature is used, by about 25 K, in the region of lowest  $E^*$ .

Fig. 23 also shows  $E^*$  levels significantly less than in the PC flue gas case. This is due largely to the smaller amount of  $\text{CO}_2$  that must be captured. For  $\Delta s_{\text{chem}} = -130$  J/(mol K), with two ideal absorber stages ( $N_s = 2$ ), and best-case values of other process parameters ( $T_{\text{cw}} = 293.15$  K,  $\Delta T_{\text{appr}} = 5$  K), the variation of  $E^*$  with  $\Delta h_{\text{chem}}$  on a per unit mass basis is shown in Fig. 25 (and on an absolute basis in Fig. 22). Near the optimal  $\Delta h_{\text{chem}}$  value for NGCC (about  $-52$  kJ/mol), the parasitic energy per unit mass of  $\text{CO}_2$  captured is only slightly higher than in the PC flue gas case. The optimal  $E^*$  value (Fig. 22) is 37 MWe. As in the PC flue gas case, this value differs from standard carbon capture technology largely in the heat requirement  $Q_s$ , which is 88 MWth for the case considered here and 189 MWth for Case 14 in the DOE/NETL study,<sup>50</sup> which uses the Econamine FG Plus<sup>SM</sup> process. On a per metric ton of  $\text{CO}_2$  captured

basis, these heat requirements become 1.73 GJ/t for the case considered here and 3.74 GJ/t for DOE/NETL Case 14.

### 4.3 Two-site chemical absorption

We now consider the case of a two-site IL absorbent, as described in Section 2.3. For the case of PC flue gas, the variation in the optimal parasitic energy  $E^*$  with the site absorption enthalpies,  $\Delta h_{\text{chem},1}$  and  $\Delta h_{\text{chem},2}$ , is shown in Fig. 26, assuming  $\Delta s_{\text{chem}} = \Delta s_{\text{chem},1} = \Delta s_{\text{chem},2} = -130$  J/(mol K), with other sensitivity parameters held at their base values (Table 2). As above, each point on this plot represents an optimization problem in which  $E$  was optimized with respect to the absorber and stripper conditions,  $T_a$ ,  $P_a$ ,  $T_s$ , and  $P_s$ , to determine  $E^*$ . The plot shows a “valley” of low  $E^*$  values running from the center of the plot towards the lower right, roughly along the line  $\Delta h_{\text{chem},1} + \Delta h_{\text{chem},2} = -98$  kJ/mol. As one moves along this line to the lower right,  $\Delta h_{\text{chem},2}$  becomes increasing larger in magnitude than  $\Delta h_{\text{chem},1}$ , indicating a growing cooperative binding effect. The isotherm inflection point that is characteristic of cooperative binding will occur when  $\Delta h_{\text{chem},2} - \Delta h_{\text{chem},1} < RT \ln 2 \approx 1.75$  kJ/mol @ 303.15 K (see Supporting Information). Unlike the one-site cases, the region of lowest  $E^*$  values also corresponds closely to the region of highest cyclic capacity, as shown in Fig. 27.

Along the optimal valley, from about  $(\Delta h_{\text{chem},1}, \Delta h_{\text{chem},2}) = (-45, -53)$  to  $(-20, -78)$  kJ/mol, the optimal absorber conditions are at their default minimum values of  $T_a = 313.15$  K and  $P_a = 1$  bar, and the optimal stripper conditions are  $T_s$  in the range of 455 K to 457 K and  $P_s$  in the range of 5.1 to 5.7 bar. The lowest  $E^*$  level for the two-site case is about 100 MWe. For the one-site case with the same base parameter values, the lowest  $E^*$  level was about 119 MWe (Fig. 9 at  $\Delta s_{\text{chem}} = -130$  J/(mol K)). The reduction in parasitic energy in the two-site case is due primarily to the ability to use an increased pressure in the stripper, resulting in lower CO<sub>2</sub> compression costs. The increased stripper pressure is possible because of the cooperative binding effect. This can be seen in Fig. 28, which shows the absorption isotherms at 455 K for several  $(\Delta h_{\text{chem},1}, \Delta h_{\text{chem},2})$  points on the  $\Delta h_{\text{chem},1} + \Delta h_{\text{chem},2} = -98$  kJ/mol line. These curves

demonstrate the transition into the cooperative binding regime, with the three lowest curves,  $(-48, -50)$ ,  $(-43, -65)$ , and  $(-38, -60)$  kJ/mol, exhibiting cooperative binding, as indicated by the sigmoidal shape with an inflection point and zero initial slope. Note that for these curves it is possible to obtain quite low uptakes at much higher pressures than in the cases without cooperative binding. For example, when  $(\Delta h_{\text{chem},1}, \Delta h_{\text{chem},2}) = (-58, -40)$  kJ/mol (no cooperative binding), reducing the uptake to 0.2 would require reducing the pressure to about 0.5 bar. However, when  $(\Delta h_{\text{chem},1}, \Delta h_{\text{chem},2}) = (-38, -60)$  kJ/mol (cooperative binding), an uptake of 0.2 or less can be achieved at pressures up to about 5 bar. Thus, cooperative binding enables the use of higher pressure in the stripper, with accompanying savings in compression energy.

#### 4.4 Effect of water absorption

In the foregoing, we have assumed that no water is absorbed by the AHA solvent. However, it is known that water is soluble in AHAs,<sup>63</sup> so the potential impact of water absorption must be considered. A direct impact of water absorption is an increased heating requirement, needed to heat the water from the absorber to the stripper temperature and to overcome the heat of absorption of water into the AHA. However, there is currently no vapor-liquid equilibrium data available for water vapor and AHAs, nor is there data for the enthalpy and entropy of absorption of water vapor into AHAs. Thus, to roughly bound the potential additional heating required by water absorption, we will assume that *all* the water vapor entering the absorber is absorbed, and that the heat of absorption is  $-30$  kJ/mol, a figure measured<sup>101</sup> for the absorption of water vapor into the IL [bmim][PF<sub>6</sub>]. With these assumptions, and taking  $N_s = 2$ ,  $T_{\text{cw}} = 293.15$  K, and  $\Delta T_{\text{appr}} = 5$  K, the additional energy required for the PC flue gas case is 6.2 MWe, about a 6% increase over the 107 MWe required for the case without water absorption. For the NGCC flue gas, the additional energy required is 8.5 MWe, about a 23% increase over the 37 MWe required for the no water absorbed case. The impact of water absorption is larger in the NGCC case because a higher stripper temperature is used, thus increasing the sensible heat needed and increasing the power equivalence factor, and because of the higher water content of the flue gas relative to CO<sub>2</sub> content. In these rough upper bounds on the additional heating required due to water, the heat of water desorption is the predominant contribution, accounting for 86% of the total in the PC case and 82% in the NGCC case. Depending on the actual amount

of water absorbed for a specific AHA, it may be desirable to consider removing additional water from the flue gas before contact with the AHA in the absorber. In any case, almost all water must be removed at some point prior to compression and transport of the CO<sub>2</sub> product. Use of a glycol-based dehydration or solid bed desiccant unit is a common suggestion for this purpose.

Other potential effects of water absorption have been studied in some detail by Seo et al.<sup>63</sup> for the specific AHA [P<sub>66614</sub>][2-CNpyr], with focus on effects of water on liquid viscosity, CO<sub>2</sub> uptake, and anion reprotonation. Addition of water to pure [P<sub>66614</sub>][2-CNpyr] reduces its viscosity; however, addition of water to [P<sub>66614</sub>][2-CNpyr] complexed with CO<sub>2</sub> increases the viscosity initially but eventually decreases the viscosity as more water is added. While we have not considered viscous effects here, viscosity is clearly an important factor in determining mass transfer rates and absorber hydrodynamics, factors that will be considered in a rate-based model of AHA-based CO<sub>2</sub> capture to be presented elsewhere. Seo et al.<sup>63</sup> also have observed that, for [P<sub>66614</sub>][2-CNpyr], the absorption of water enhances the uptake of CO<sub>2</sub> at low CO<sub>2</sub> partial pressure. This is attributed to water molecules interacting differently with the AHA-CO<sub>2</sub> complex as compared to the uncomplexed AHA, thereby making their activity coefficients different. If the activity coefficient of the complexed AHA is reduced relative to the uncomplexed AHA then this will drive the equilibrium for the reaction given by Eq. (1) to the right, increasing the CO<sub>2</sub> uptake. Finally, there is the potential for reprotonation of the AHA anion in the presence of water. Anion reprotonation, resulting in formation of a neutral species and inactivation of CO<sub>2</sub> binding capacity, is known to be an issue in the case of amino-acid-based ILs.<sup>62,102</sup> However, NMR studies by Seo et al.<sup>63</sup> have shown that, for [P<sub>66614</sub>][2-CNpyr], anion reprotonation does not appear to be an issue. While these effects of water on the AHA [P<sub>66614</sub>][2-CNpyr] have been studied, the effect of water absorption on other AHAs is not well known and is the subject of current study.

## 5. Concluding Remarks

The tunability of aprotic heterocyclic anion ILs, or AHAs, especially with respect to their binding energy with CO<sub>2</sub>, is an attractive feature, but presents a materials design challenge. In this work, we have established a simple process model of CO<sub>2</sub> capture from post-combustion flue gas, and formulated the challenge as a type of simultaneous materials and process design problem, in which flowrates, heat duties, and process conditions that minimize a simple energy

usage objective function are determined. By studying the sensitivity of this optimum with respect to various material properties and process parameters, materials property targets were identified. For flue gas from pulverized coal power plants, these results indicate that for  $-140 \leq \Delta s_{\text{chem}} \leq -120$  J/(mol K), there is a target range of optimal chemical absorption strength of about  $-54$  to  $-48$  kJ/mol. If this target cannot be met, it is preferable to miss on the too strong (more negative) side. For flue gas from natural gas combined cycle power plants, the target range becomes stronger by about 4 kJ/mol. Some AHAs having  $\Delta h_{\text{chem}}$  values in the desired ranges have already been indentified.<sup>63</sup> With these targets known, other promising absorbents may be sought using quantum chemical calculations to design appropriate AHA molecules, thus determining candidates for laboratory synthesis and characterization. The model used here is based on equilibrium considerations, and does not account for viscous losses or rate effects. However, we are also developing a rate-based model of CO<sub>2</sub> capture using AHAs, and results of its application will be presented elsewhere.

**Acknowledgements.** This work has been supported by the University of Notre Dame Strategic Energy Initiative and by the Stanford University Global Climate and Energy Project under Activity Number 73. We thank Professor Brandon L. Ashfeld, Professor Haifeng Gao and Dr. Doyun Lee for the synthesis of trihexyl(tetradecyl)phosphonium 2-(1H-pyrrol-2-ylmethyl)pyrrolide ([P<sub>66614</sub>][PMP]). We also thank Dr. M. Aruni DeSilva for the synthesis of tetrabutylphosphonium 6-bromo-benzimidazolide ([P<sub>4444</sub>][6-BrBnim]), and trihexyl(tetradecyl)phosphonium 2-(cyano)pyrrolide ([P<sub>66614</sub>][2-CNpyr]) and Dr. Mauricio Quiroz-Guzman for the synthesis of tetrabutylphosphonium 3-trifluoromethylpyrazolide ([P<sub>4444</sub>][3-CF<sub>3</sub>pyra]).

## References

- (1) Figueroa, J. D.; Fout, T.; Plasynski, S.; McIlvried, H.; Srivastava, R. D. Advances in CO<sub>2</sub> Capture Technology—The U.S. Department of Energy’s Carbon Sequestration Program. *Int. J. Greenhouse Gas Control* **2008**, *2*, 9-20.
- (2) Yang, H.; Xu, Z.; Fan, M.; Gupta, R.; Slimane, R. B.; Bland, A. E.; Wright, I. Progress in Carbon Dioxide Separation and Capture: A Review. *J. Environ. Sci.* **2008**, *20*, 14-27.

- (3) Rochelle, G. T. Amine Scrubbing for CO<sub>2</sub> Capture. *Science* **2009**, 325, 1652-1654.
- (4) Olajire, A. A. CO<sub>2</sub> Capture and Separation Technologies for End-of-Pipe Applications – A Review. *Energy* **2010**, 35, 2610-2628.
- (5) Brunetti, A.; Scura, F.; Barbieri, G.; Drioli, E. Membrane Technologies for CO<sub>2</sub> Separation. *J. Membr. Sci.* **2010**, 359, 115-125.
- (6) MacDowell, N.; Florin, N.; Buchard, A.; Hallett, J.; Galindo, A.; Jackson, G.; Adjiman, C. S.; Williams, C. K.; Shah, N.; Fennell, P. An Overview of CO<sub>2</sub> Capture Technology. *Energy Environ. Sci.* **2010**, 3, 1645-1669.
- (7) Li, J.; Ma, Y.; McCarthy, M. C.; Sculley, J.; Yu, J.; Jeong, H.; Balbuena, P. B.; Zhou, H. Carbon Dioxide Capture-Related Gas Adsorption and Separation in Metal-Organic Frameworks. *Coord. Chem. Rev.* **2011**, 255, 1791-1823.
- (8) Pires, J. C. M.; Martins, F. G.; Alvim-Ferraz, M. C. M.; Simões, M. Recent Developments on Carbon Capture and Storage: An Overview. *Chem. Eng. Res. Des.* **2011**, 89, 1446-1460.
- (9) Quintella, C. M.; Hatimondi, S. A.; Musse, A. P. S.; Miyazaki, S. F.; Cerqueira, G. S.; de Araujo Moreira, A. CO<sub>2</sub> Capture Technologies: An Overview with Technology Assessment Based on Patents and Articles. *Energy Procedia* **2011**, 4, 2050-2057.
- (10) Wang, M.; Lawal, A.; Stephenson, P.; Sidders, J.; Ramshaw, C. Post-Combustion CO<sub>2</sub> Capture with Chemical Absorption: A State-of-the-Art Review. *Chem. Eng. Res. Des.* **2011**, 89, 1609-1624.
- (11) Fu, C.; Gundersen, T. Carbon Capture and Storage in the Power Industry: Challenges and Opportunities. *Energy Procedia* **2012**, 16, Part C, 1806-1812.
- (12) Luis, P.; Van Gerven, T.; Van der Bruggen, B. Recent Developments in Membrane-Based Technologies for CO<sub>2</sub> Capture. *Prog. Energy Combust. Sci.* **2012**, 38, 419-448.
- (13) Kuramochi, T.; Ramírez, A.; Turkenburg, W.; Faaij, A. Comparative Assessment of CO<sub>2</sub> Capture Technologies for Carbon-Intensive Industrial Processes. *Prog. Energy Combust. Sci.* **2012**, 38, 87-112.
- (14) Yu, C. H.; Huang, C. H.; Tan, C. S. A Review of CO<sub>2</sub> Capture by Absorption and Adsorption. *Aerosol Air Qual. Res.* **2012**, 12, 745-769.
- (15) Mondal, M. K.; Balsora, H. K.; Varshney, P. Progress and Trends in CO<sub>2</sub> Capture/Separation Technologies: A Review. *Energy* **2012**, 46, 431-441.
- (16) Rubin, E. S.; Mantripragada, H.; Marks, A.; Versteeg, P.; Kitchin, J. The Outlook for Improved Carbon Capture Technology. *Prog. Energy Combust. Sci.* **2012**, 38, 630-671.

- (17) Liu, Y.; Wang, Z. U.; Zhou, H. -. Recent Advances in Carbon Dioxide Capture with Metal-Organic Frameworks. *Greenhouse Gases: Sci. Technol.* **2012**, *2*, 239-259.
- (18) Samanta, A.; Zhao, A.; Shimizu, G. K. H.; Sarkar, P.; Gupta, R. Post-Combustion CO<sub>2</sub> Capture using Solid Sorbents: A Review. *Ind. Eng. Chem. Res.* **2012**, *51*, 1438-1463.
- (19) Li, L.; Zhao, N.; Wei, W.; Sun, Y. A Review of Research Progress on CO<sub>2</sub> Capture, Storage, and Utilization in Chinese Academy of Sciences. *Fuel* **2013**, *108*, 112-130.
- (20) Li, B.; Duan, Y.; Luebke, D.; Morreale, B. Advances in CO<sub>2</sub> Capture Technology: A Patent Review. *Appl. Energy* **2013**, *102*, 1439-1447.
- (21) Chen, Z.; Deng, S.; Wei, H.; Wang, B.; Huang, J.; Yu, G. Activated Carbons and Amine-Modified Materials for Carbon Dioxide Capture — A Review. *Front. Environ. Sci. Eng.* **2013**, *7*, 326-340.
- (22) Zaman, M.; Lee, J. Carbon Capture from Stationary Power Generation Sources: A Review of the Current Status of the Technologies. *Korean J. Chem. Eng.* **2013**, *30*, 1497-1526.
- (23) Yeo, Z. Y.; Chew, T. L.; Zhu, P. W.; Mohamed, A. R.; Chai, S. P. Synthesis and Performance of Microporous Inorganic Membranes for CO<sub>2</sub> Separation: A Review. *J. Porous Mater.* **2013**, *20*, 1457-1475.
- (24) Satish, K.; Cho, J. H.; Moon, L. Ionic Liquid-Amine Blends and CO<sub>2</sub>BOLs: Prospective Solvents for Natural Gas Sweetening and CO<sub>2</sub> Capture Technology--A Review. *Int. J. Greenhouse Gas Control* **2014**, *20*, 87-116.
- (25) Belaissaoui, B.; Favre, E. Membrane Separation Processes for Post-Combustion Carbon Dioxide Capture: State of the Art and Critical Overview. *Oil Gas Sci. Technol.* **2014**, *60*, 1005-1020.
- (26) Wang, J. Y.; Huang, L.; Yang, R. Y.; Zhang, Z.; Wu, J. W.; Gao, Y. S.; Wang, Q.; O'Hare, D.; Zhong, Z. Y. Recent Advances in Solid Sorbents for CO<sub>2</sub> Capture and New Development Trends. *Energy Environ. Sci.* **2014**, *7*, 3478-3518.
- (27) Leung, D. Y. C.; Caramanna, G.; Maroto-Valer, M. M. An Overview of Current Status of Carbon Dioxide Capture and Storage Technologies. *Renewable Sustainable Energy Rev.* **2014**, *39*, 426-443.
- (28) Yang, N.; Yu, H.; Li, L. C.; Xu, D. Y.; Han, W. F.; Feron, P. Aqueous Ammonia (NH<sub>3</sub>) Based Post Combustion CO<sub>2</sub> Capture: A Review. *Oil Gas Sci. Technol.* **2014**, *69*, 931-945.
- (29) Zhang, Z. J.; Yao, Z. Z.; Xiang, S. C.; Chen, B. L. Perspective of Microporous Metal-Organic Frameworks for CO<sub>2</sub> Capture and Separation. *Energy Environ. Sci.* **2014**, *7*, 2868-2899.

- (30) Sabouni, R.; Kazemian, H.; Rohani, S. Carbon Dioxide Capturing Technologies: A Review Focusing on Metal Organic Framework Materials (MOFs). *Environ. Sci. Pollut. Res.* **2014**, *21*, 5427-5449.
- (31) Gargiulo, N.; Pepe, F.; Caputo, D. CO<sub>2</sub> Adsorption by Functionalized Nanoporous Materials: A Review. *J. Nanosci. Nanotechnol.* **2014**, *14*, 1811-1822.
- (32) Chen, C.; Kim, J.; Ahn, W. CO<sub>2</sub> Capture by Amine-Functionalized Nanoporous Materials: A Review. *Korean J. Chem. Eng.* **2014**, *31*, 1919-1934.
- (33) Boot-Handford, M. E.; Abanades, J. C.; Anthony, E. J.; Blunt, M. J.; Brandani, S.; Mac Dowell, N.; Fernandez, J. R.; Ferrari, M. C.; Gross, R.; Hallett, J. P.; Haszeldine, R. S.; Heptonstall, P.; Lyngfelt, A.; Makuch, Z.; Mangano, E.; Porter, R. T. J.; Pourkashanian, M.; Rochelle, G. T.; Shah, N.; Yao, J. G.; Fennell, P. S. Carbon Capture and Storage Update. *Energy Environ. Sci.* **2014**, *7*, 130-189.
- (34) Babamohammadi, S.; Shamiri, A.; Aroua, M. K. A Review of CO<sub>2</sub> Capture by Absorption in Ionic Liquid-Based Solvents. *Rev. Chem. Eng.* **2015**, *31*, 383-412.
- (35) Budzianowski, W. M. Single Solvents, Solvent Blends, and Advanced Solvent Systems in CO<sub>2</sub> Capture by Absorption: A Review. *Int. J. Global Warming* **2015**, *7*, 184-225.
- (36) Khalilpour, R.; Mumford, K.; Zhai, H.; Abbas, A.; Stevens, G.; Rubin, E. S. Membrane-Based Carbon Capture from Flue Gas: A Review. *J. Cleaner Prod.* **2015**, *103*, 286-300.
- (37) Koronaki, I. P.; Prentza, L.; Papaefthimiou, V. Modeling of CO<sub>2</sub> Capture Via Chemical Absorption Processes – An Extensive Literature Review. *Renewable Sustainable Energy Rev.* **2015**, *50*, 547-566.
- (38) Lee, S.; Park, S. A Review on Solid Adsorbents for Carbon Dioxide Capture. *J. Ind. Eng. Chem.* **2015**, *23*, 1-11.
- (39) Shakerian, F.; Kim, K.; Szulejko, J. E.; Park, J. A Comparative Review between Amines and Ammonia as Sorptive Media for Post-Combustion CO<sub>2</sub> Capture. *Appl. Energy* **2015**, *148*, 10-22.
- (40) Mumford, K. A.; Wu, Y.; Smith, K. H.; Stevens, G. W. Review of Solvent Based Carbon-Dioxide Capture Technologies. *Front. Chem. Sci. Eng.* **2015**, *9*, 125-141.
- (41) Wang, M.; Joel, A. S.; Ramshaw, C.; Eimer, D.; Musa, N. M. Process Intensification for Post-Combustion CO<sub>2</sub> Capture with Chemical Absorption: A Critical Review. *Appl. Energy* **2015**, *158*, 275-291.
- (42) Mirzaei, S.; Shamiri, A.; Aroua, M. K. A Review of Different Solvents, Mass Transfer, and Hydrodynamics for Postcombustion CO<sub>2</sub> Capture. *Rev. Chem. Eng.* **2015**, *31*, 521-561.

- (43) Ben-Mansour, R.; Habib, M. A.; Bamidele, O. E.; Basha, M.; Qasem, N. A. A.; Peedikakkal, A.; Laoui, T.; Ali, M. Carbon Capture by Physical Adsorption: Materials, Experimental Investigations and Numerical Modeling and Simulations - A Review. *Appl. Energy* **2016**, *161*, 225-255.
- (44) Liang, Z.; Fu, K.; Idem, R.; Tontiwachwuthikul, P. Review on Current Advances, Future Challenges and Consideration Issues for Post-Combustion CO<sub>2</sub> Capture using Amine-Based Absorbents. *Chin. J. Chem. Eng.* **2016**, *24*, 278-288.
- (45) Wiheeb, A. D.; Helwani, Z.; Kim, J.; Othman, M. R. Pressure Swing Absorption Technologies for Carbon Capture. *Sep. Purif. Rev.* **2016**, *45*, 108-121.
- (46) Gurkan, B.; Goodrich, B. F.; Mindrup, E. M.; Ficke, L. E.; Massel, M.; Seo, S.; Senftle, T. P.; Wu, H.; Glaser, M. F.; Shah, J. K.; Maginn, E. J.; Brennecke, J. F.; Schneider, W. F. Molecular Design of High Capacity, Low Viscosity, Chemically Tunable Ionic Liquids for CO<sub>2</sub> Capture. *J. Phys. Chem. Lett.* **2010**, *1*, 3494-3499.
- (47) Chowdhury, F. A.; Yamada, H.; Higashii, T.; Goto, K.; Onoda, M. CO<sub>2</sub> Capture by Tertiary Amine Absorbents: A Performance Comparison Study. *Ind. Eng. Chem. Res.* **2013**, *52*, 8323-8331.
- (48) Chen, X.; Rochelle, G. T. Aqueous Piperazine Derivatives for CO<sub>2</sub> Capture: Accurate Screening by a Wetted Wall Column. *Chem. Eng. Res. Des.* **2011**, *89*, 1693-1710.
- (49) Oyenekan, B. A.; Rochelle, G. T. Alternative Stripper Configurations for CO<sub>2</sub> Capture by Aqueous Amines. *AIChE J.* **2007**, *53*, 3144-3154.
- (50) Haslbeck, J. L.; Kuehn, N. J.; Lewis, E. G.; Pinkerton, L. L.; Simpson, J.; Turner, M. J.; Varghese, E.; Woods, M. C. Cost and Performance Baseline for Fossil Energy Plants, Volume 1: Bituminous Coal and Natural Gas to Electricity, Revision 2a. Report DOE/NETL-2010/1397, National Energy Technology Laboratory, 2013.
- (51) Fout, T.; Zoelle, A.; Keairns, D.; Turner, M.; Woods, M.; Keuhn, N.; Shah, V.; Chou, V.; Pinkerton, L. Cost and Performance Baseline for Fossil Energy Plants, Volume 1a: Bituminous Coal (PC) and Natural Gas to Electricity, Revision 3. Report DOE/NETL-2015/1723, National Energy Technology Laboratory, 2015.
- (52) Ramdin, M.; de Loos, T. W.; Thijs J.H.; Vlugt, T. J. H. State-of-the-Art of CO<sub>2</sub> Capture with Ionic Liquids. *Ind. Eng. Chem. Res.* **2012**, *51*, 8149-8177.
- (53) Zhang, X.; Zhang, X.; Dong, H.; Zhao, Z.; Zhang, S.; Huang, Y. Carbon Capture with Ionic Liquids: Overview and Progress. *Energy Environ. Sci.* **2012**, *5*, 6668-6681.
- (54) Zhao, Z.; Dong, H.; Zhang, X. The Research Progress of CO<sub>2</sub> Capture with Ionic Liquids. *Chin. J. Chem. Eng.* **2012**, *20*, 120-129.

- (55) Zhang, L.; Chen, J.; Lv, J. X.; Wang, S. F.; Cui, Y. Progress and Development of Capture for CO<sub>2</sub> by Ionic Liquids. *Korean J. Chem. Eng.* **2013**, *25*, 2355-2358.
- (56) Gonzalez-Miquel, M.; Bedia, J.; Abrusci, C.; Palomar, J.; Rodriguez, F. Anion Effects on Kinetics and Thermodynamics of CO<sub>2</sub> Absorption in Ionic Liquids. *J. Phys. Chem. B* **2013**, *117*, 3398-3406.
- (57) Anderson, J. L.; Dixon, J. K.; Brennecke, J. F. Solubility of CO<sub>2</sub>, CH<sub>4</sub>, C<sub>2</sub>H<sub>6</sub>, C<sub>2</sub>H<sub>4</sub>, O<sub>2</sub>, and N<sub>2</sub> in 1-Hexyl-3-Methylpyridinium Bis(Trifluoromethylsulfonyl)Imide: Comparison to Other Ionic Liquids. *Acc. Chem. Res.* **2007**, *40*, 1208-1216.
- (58) Davis, J. Task-Specific Ionic Liquids. *Chem. Lett.* **2004**, *33*, 1072-1077.
- (59) Bates, E. D.; Mayton, R. D.; Ntai, I.; Davis, J. H. CO<sub>2</sub> Capture by a Task-Specific Ionic Liquid. *J. Am. Chem. Soc.* **2002**, *124*, 926.
- (60) Gutowski, K. E.; Maginn, E. J. Amine-Functionalized Task-Specific Ionic Liquids: A Mechanistic Explanation for the Dramatic Increase in Viscosity upon Complexation with CO<sub>2</sub> from Molecular Simulation. *J. Am. Chem. Soc.* **2008**, *130*, 14690-14704.
- (61) Mindrup, E.; Schneider, W. F. Computational Comparison of Tethering Strategies for Amine Functionalized Ionic Liquids. *ACS Symp. Ser.* **2010**, *1030*, 419-430.
- (62) Goodrich, B. F.; de la Fuente, J. C.; Gurkan, B. E.; Lopez, Z. K.; Price, E. A.; Huang, Y.; Brennecke, J. F. Effect of Water and Temperature on Absorption of CO<sub>2</sub> by Amine-Functionalized Anion-Tethered Ionic Liquids. *J. Phys. Chem. B* **2011**, *115*, 9140-9150.
- (63) Seo, S.; Quiroz-Guzman, M.; DeSilva, M. A.; Lee, T. B.; Huang, Y.; Goodrich, B. F.; Schneider, W. F.; Brennecke, J. F. Chemically Tunable Ionic Liquids with Aprotic Heterocyclic Anion (AHA) for CO<sub>2</sub> Capture. *J. Phys. Chem. B* **2014**, *118*, 5740-5751.
- (64) Seo, S.; DeSilva, M. A.; Xia, H.; Brennecke, J. F. Effect of Cation on Physical Properties and CO<sub>2</sub> Solubility for Phosphonium-Based Ionic Liquids with 2-Cyanopyrrolide Anions. *J. Phys. Chem. B* **2015**, *119*, 11807-11814.
- (65) Eden, M. R.; Jørgensen, S. B.; Gani, R.; El-Halwagi, M. M. A Novel Framework for Simultaneous Separation Process and Product Design. *Chem. Eng. Process.* **2004**, *43*, 595-608.
- (66) Martín, M.; Martínez, A. A Methodology for Simultaneous Process and Product Design in the Formulated Consumer Products Industry: The Case Study of the Detergent Business. *Chem. Eng. Res. Des.* **2013**, *91*, 795-809.
- (67) Gani, R.; Brignole, E. A. Molecular Design of Solvents for Liquid Extraction Based on UNIFAC. *Fluid Phase Equilib.* **1983**, *13*, 331-340.

- (68) Lek-utaiwana, P.; Suphanitb, B.; Douglas, P. L.; Mongkolsiri, N. Design of Extractive Distillation for the Separation of Close-Boiling Mixtures: Solvent Selection and Column Optimization. *Comput. Chem. Eng.* **2011**, *35*, 1088-1100.
- (69) Papadopoulos, A. I.; Linke, P. Multiobjective Molecular Design for Integrated Process-Solvent Systems Synthesis. *AIChE J.* **2006**, *52*, 1057-1070.
- (70) Harini, M.; Adhikari, J.; Rani, K. Y. A Review on Property Estimation Methods and Computational Schemes for Rational Solvent Design: A Focus on Pharmaceuticals. *Ind. Eng. Chem. Res.* **2013**, *52*, 6869-6893.
- (71) Zhou, T.; Zhou, Y.; Sundmacher, K. A Hybrid Stochastic-Deterministic Optimization Approach for Integrated Solvent and Process Design. *Chem. Eng. Sci.* **2016**, *in press*.
- (72) Roughton, B. C.; Christian, B.; White, J.; Camarda, K. V.; Gani, R. Simultaneous Design of Ionic Liquid Entrainers and Energy Efficient Azeotropic Separation Processes. *Comput. Chem. Eng.* **2012**, *42*, 248-262.
- (73) Kazantzi, V.; Qin, X.; El-Halwagi, M.; Eljack, F.; Eden, M. Simultaneous Process and Molecular Design through Property Clustering Techniques: A Visualization Tool. *Ind. Eng. Chem. Res.* **2007**, *46*, 3400-3409.
- (74) Chemmangattuvalappil, N. G.; Solvason, C. C.; Bommareddy, S.; Eden, M. R. Combined Property Clustering and GC+ Techniques for Process and Product Design. *Comput. Chem. Eng.* **2010**, *34*, 582-591.
- (75) McLeese, S. E.; Eslick, J. C.; Hoffmann, N. J.; Scurto, A. M.; Camarda, K. V. Design of Ionic Liquids Via Computational Molecular Design. *Comput. Chem. Eng.* **2010**, *34*, 1476-1480.
- (76) Pereira, F. E.; Keskes, E.; Galindo, A.; Jackson, G.; Adjiman, C. S. Integrated Solvent and Process Design using a SAFT-VR Thermodynamic Description: High-Pressure Separation of Carbon Dioxide and Methane. *Comput. Chem. Eng.* **2011**, *35*, 474-491.
- (77) Oyarzúna, B.; Bardowa, A.; Grossa, J. Integration of Process and Solvent Design Towards a Novel Generation of CO<sub>2</sub> Absorption Capture Systems. *Energy Procedia* **2011**, *4*, 282-290.
- (78) Burger, J.; Papaioannou, V.; Gopinath, S.; Jackson, G.; Galindo, A.; Adjiman, C. S. A Hierarchical Method to Integrated Solvent and Process Design of Physical CO<sub>2</sub> Absorption using the SAFT-Gamma Mie Approach. *AIChE J.* **2015**, *61*, 3249-3269.
- (79) Chong, F. K.; Chemmangattuvalappil, N. G.; Eljack, F. T.; Atilhan, M.; Foo, D. C. Y. Designing Ionic Liquid Solvents for Carbon Capture using Property-Based Visual Approach. *Clean Technol. Environ. Policy* **2016**, *18*, 1177-1188.
- (80) Hada, S.; Herring III, R. H.; Davis, S. E.; Eden, M. R. Multivariate Characterization, Modeling, and Design of Ionic Liquid Molecules. *Comput. Chem. Eng.* **2015**, *81*, 310-322.

- (81) Kumelan, J.; Kamps, I.; Tuma, D.; Maurer, G.; Kumelan, J. Solubility of CO<sub>2</sub> in the Ionic Liquid [Hmim][Tf<sub>2</sub>N]. *J. Chem. Thermodyn.* **2006**, *38*, 1396-1401.
- (82) Carvalho, P.; Carvalho, P. J. On the Nonideality of CO<sub>2</sub> Solutions in Ionic Liquids and Other Low Volatile Solvents. *J. Phys. Chem. Lett.* **2010**, *1*, 774-780.
- (83) Brennecke, J.; Gurkan, B. Ionic Liquids for CO<sub>2</sub> Capture and Emission Reduction. *J. Phys. Chem. Lett.* **2010**, *1*, 3459-3464.
- (84) Aki, S.; Mellein, B.; Saurer, E.; Brennecke, J. High-Pressure Phase Behavior of Carbon Dioxide with Imidazolium-Based Ionic Liquids. *J. Phys. Chem. B* **2004**, *108*, 20355-20365.
- (85) Anthony, J. L.; Anderson, J. L.; Maginn, E. J.; Brennecke, J. F. Anion Effects on Gas Solubility in Ionic Liquids. *J. Phys. Chem. B* **2005**, *109*, 6366-6374.
- (86) Muldoon, M. J.; Aki, S. N. V. K.; Anderson, J. L.; Dixon, J. K.; Brennecke, J. F. Improving Carbon Dioxide Solubility in Ionic Liquids. *J. Phys. Chem. B* **2007**, *111*, 9001-9009.
- (87) Shiflett, M. B.; Yokozeki, A. Phase Behavior of Carbon Dioxide in Ionic Liquids: [Emim][Acetate], [Emim][Trifluoroacetate], and [Emim][Acetate] + [Emim][Trifluoroacetate] Mixtures. *J. Chem. Eng. Data* **2009**, *54*, 108-114.
- (88) Leeder, J. D.; Watt, I. C. The Role of Amino Groups in Water Absorption by Keratin. *J. Phys. Chem.* **1965**, *69*, 3280-3284.
- (89) Bennett, J. E. Acid Gas and Nitrogen Solubility in Ionic Liquids for Carbon Capture Applications, Ph.D. Thesis, University of Notre Dame, Notre Dame, Indiana, USA, 2014.
- (90) Massel, M. Thermodynamic and Thermophysical Properties of Ionic Liquid Mixtures, Ph.D. Thesis, University of Notre Dame, Notre Dame, Indiana, USA, 2014.
- (91) Shiflett, M. B.; Drew, D. W.; Cantini, R. A.; Yokozeki, A. Carbon Dioxide Capture Using Ionic Liquid 1-Butyl-3-Methylimidazolium Acetate. *Energy Fuels* **2010**, *24*, 5781-5789.
- (92) Khonkaen, K.; Siemanond, K.; Henni, A. Simulation of Carbon Dioxide Capture Using Ionic Liquid 1-Ethyl-3-Methylimidazolium Acetate. *Comput.-Aided Chem. Eng.* **2014**, *33*, 1045-1050.
- (93) Linstrom, P. J.; Mallard, W. G., Eds. *NIST Chemistry WebBook, NIST Standard Reference Database Number 69*. National Institute of Standards and Technology: Gaithersburg, MD, <http://webbook.nist.gov> (retrieved, January 6, 2016).
- (94) Crosthwaite, J. M.; Muldoon, M. J.; Dixon, J. K.; Anderson, J. L.; Brennecke, J. F. Phase Transition and Decomposition Temperatures, Heat Capacities and Viscosities of Pyridinium Ionic Liquids. *J. Chem. Thermodyn.* **2005**, *37*, 559-568.

- (95) McCollum, D. L.; Ogden, J. M. Techno-Economic Models for Carbon Dioxide Compression, Transport, and Storage & Correlations for Estimating Carbon Dioxide Density and Viscosity. Report UCD-ITS-RR-06-14, Institute for Transportation Studies, University of California, Davis, 2006.
- (96) Peeters, A. N. M.; Faaij, A. P. C.; Turkenburg, W. C. Techno-Economic Analysis of Natural Gas Combined Cycles with Post-Combustion CO<sub>2</sub> Absorption, Including a Detailed Evaluation of the Development Potential. *Int. J. Greenhouse Gas Control* **2007**, *1*, 396-417.
- (97) Lucquiaud, M.; Gibbins, J. On the Integration of CO<sub>2</sub> Capture with Coal-Fired Power Plants: A Methodology to Assess and Optimise Solvent-Based Post-Combustion Capture Systems. *Chem. Eng. Res. Des.* **2011**, *89*, 1553-1571.
- (98) Oyenekan, B.; Rochelle, G. Energy Performance of Stripper Configurations for CO<sub>2</sub> Capture by Aqueous Amines. *Ind. Eng. Chem. Res.* **2006**, *45*, 2457-2464.
- (99) Storn, R.; Price, K. Differential Evolution – A Simple and Efficient Heuristic for Global Optimization Over Continuous Spaces. *J. Global Optim.* **1997**, *11*, 341-359.
- (100) Zhai, H.; Rubin, E. S. Systems Analysis of Ionic Liquids for Post-Combustion CO<sub>2</sub> Capture at Coal-Fired Power Plants. *Energy Procedia* **2014**, *63*, 1321-1328.
- (101) Anthony, J. L.; Maginn, E. J.; Brennecke, J. F. Solution Thermodynamics of Imidazolium-Based Ionic Liquids and Water. *J. Phys. Chem. B* **2001**, *105*, 10942-10949.
- (102) McDonald, J. L.; Sykora, R. E.; Hixon, P.; Mirjafari, A.; Davis, J. H. Impact of Water on CO<sub>2</sub> Capture by Amino Acid Ionic Liquids. *Environ. Chem. Lett.* **2014**, *12*, 201-208.

Table 1. Flue gas properties<sup>50</sup> for PC and NGCC cases.

<b>Flue Gas Properties for Subcritical Pulverized Coal (PC) Case</b>		
$P_0$	Pressure	1.0 bar
$T_0$	Temperature	57 °C
$F_0$	Total molar flow rate	111453 kmol/hr
$Y_{0,\text{CO}_2}$	Mole fraction CO <sub>2</sub>	0.1350
$Y_{0,\text{H}_2\text{O}}$	Mole fraction H <sub>2</sub> O	0.1537
$Y_{0,\text{N}_2}$	Mole fraction N <sub>2</sub>	0.6793
$Y_{0,\text{O}_2}$	Mole fraction O <sub>2</sub>	0.0238
$Y_{0,\text{Ar}}$	Mole fraction Ar	0.0081
<b>Flue Gas Properties for Natural Gas Combined Cycle (NGCC) Case</b>		
$P_0$	Pressure	1.0 bar
$T_0$	Temperature	143 °C
$F_0$	Total molar flow rate	113831 kmol/hr
$Y_{0,\text{CO}_2}$	Mole fraction CO <sub>2</sub>	0.0404
$Y_{0,\text{H}_2\text{O}}$	Mole fraction H <sub>2</sub> O	0.0867
$Y_{0,\text{N}_2}$	Mole fraction N <sub>2</sub>	0.7432
$Y_{0,\text{O}_2}$	Mole fraction O <sub>2</sub>	0.1209
$Y_{0,\text{Ar}}$	Mole fraction Ar	0.0089

Table 2. Fixed parameters (showing values), sensitivity parameters (showing base values and range studied), and decision variables (showing range constraints) for sensitivity studies reported in Section 4.

Symbol	Description [Units]	Fixed or Base Value	Range
<b>Fixed Parameters (Values)</b>			
$\Delta h_{\text{phys}}$	Enthalpy of physical absorption of CO <sub>2</sub> [kJ/mol]	-13.2	
$\Delta s_{\text{phys}}$	Entropy of physical absorption of CO <sub>2</sub> J/(mol K)	-70	
$v_{\text{AHA}}$	Molar volume of AHA [cm <sup>3</sup> /mol]	645	
$B$	AHA heat capacity parameter [J/(mol K <sup>2</sup> )]	1.89	
$C_1$	Uptake isotherm parameter for $T$ dependence	0.92	
$C_2$	Uptake isotherm parameter for $T$ dependence [K <sup>-1</sup> ]	0.0005	
<b>Sensitivity Parameters (Base Values and Range)</b>			
$\Delta h_{\text{chem}}$	Enthalpy of chemical absorption of CO <sub>2</sub> (one-site model) [kJ/mol]		[-70, -30]
$\Delta h_{\text{chem},1}$	Enthalpy of chemical absorption of CO <sub>2</sub> (first site in two-site model) [kJ/mol]		[-80, -20]
$\Delta h_{\text{chem},2}$	Enthalpy of chemical absorption of CO <sub>2</sub> (second site in two-site model) [kJ/mol]		[-80, -20]
$\Delta s_{\text{chem}}$	Entropy of chemical absorption of CO <sub>2</sub> (one-site and two-site models) [J/(mol K)]	-130	[-140, -120]
$A$	AHA heat capacity parameter [J/(mol K)]	630	[330, 930]
$T_{\text{cw}}$	Cooling water temperature [K]	303.15	[293.15, 313.15]
$\Delta T_{\text{appr}}$	Minimum approach temperature [K]	10	[5, 15]
$\Delta X_{\text{appr}}$	Approach to saturation uptake with CO <sub>2</sub> feed	0	[0, 0.2]
$N_s$	Number of equilibrium stages (absorber)	$\infty$	[1, $\infty$ ]
$\beta$	Carnot factor (integration factor)	0.75	[0.3, 1]
<b>Decision Variables (Range)</b>			
$T_a$	Absorber temperature [K]		$\geq T_{\text{cw}} + \Delta T_{\text{appr}}$
$T_s$	Stripper temperature [K]		$\leq 473.15$
$P_a$	Absorber total pressure [bar]		$\geq 1$
$P_s$	Stripper total pressure [bar]		$\geq 1$

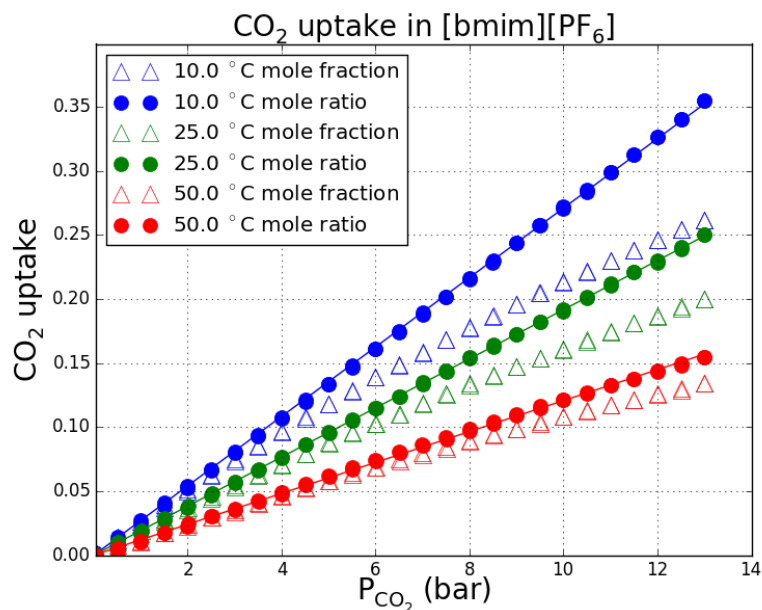


Figure 1. Physical uptake data<sup>85</sup> for [bmim][PF<sub>6</sub>], in terms of mole ratio and mole fraction, versus CO<sub>2</sub> pressure. Lines emphasize the linearity of the relationship when the mole ratio uptake scale is used. The model calculations (lines) are for  $\Delta h_{\text{phys}}^0 = -15$  kJ/mol and  $\Delta s_{\text{phys}}^0 = -84$  J/(mol K).

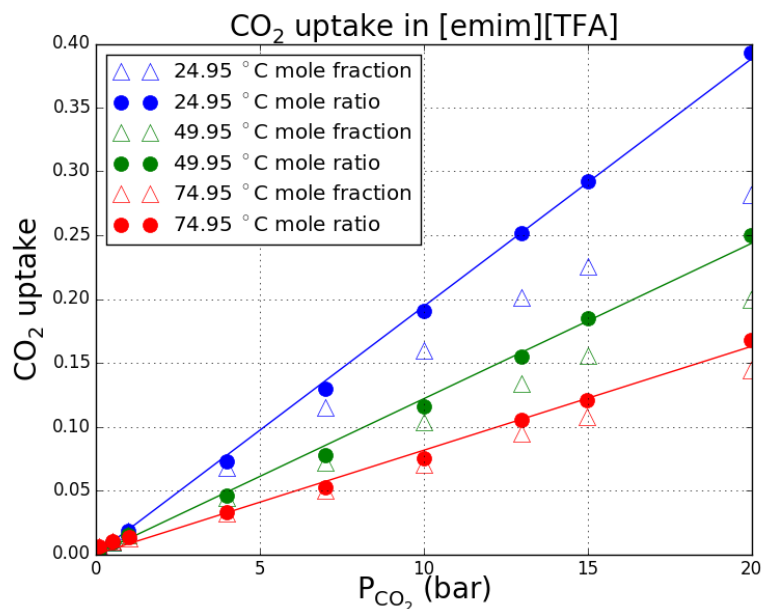


Figure 2. Physical uptake data<sup>87</sup> for 1-ethyl-3-methylimidazolium trifluoroacetate ([emim][TFA]), in terms of mole ratio and mole fraction, versus CO<sub>2</sub> pressure. Lines emphasize the linearity of the relationship when the mole ratio uptake scale is used. The model calculations (lines) are for  $\Delta h_{\text{phys}}^0 = -15$  kJ/mol and  $\Delta s_{\text{phys}}^0 = -83$  J/(mol K).

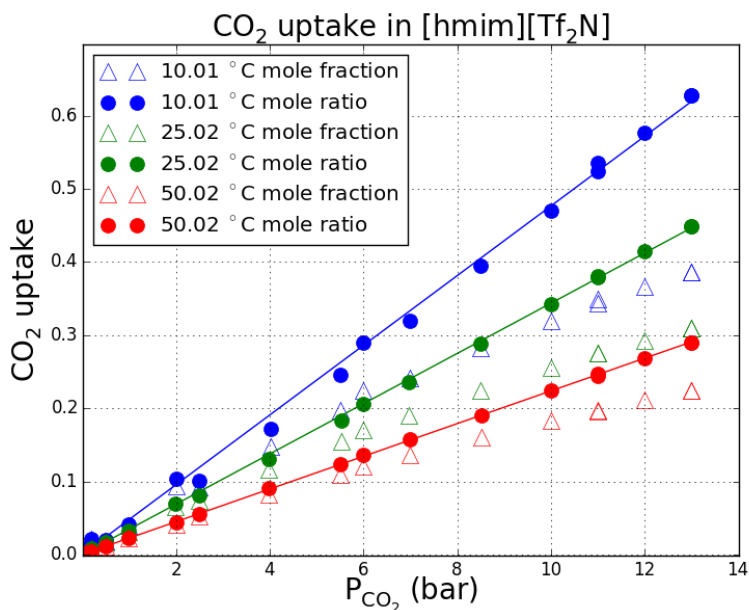


Figure 3. Physical uptake data<sup>86</sup> for [hmim][Tf<sub>2</sub>N], in terms of mole ratio and mole fraction, versus CO<sub>2</sub> pressure. Lines emphasize the linearity of the relationship when the mole ratio uptake scale is used. The model calculations (lines) are for  $\Delta h_{\text{phys}}^0 = -14$  kJ/mol and  $\Delta s_{\text{phys}}^0 = -76$  J/(mol K).

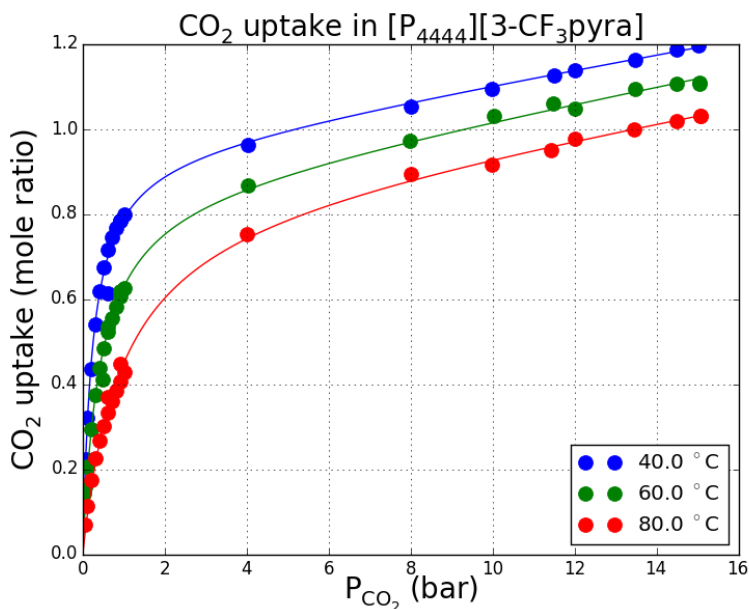


Figure 4. Experimental uptake data<sup>89</sup> for [P<sub>4444</sub>][3-CF<sub>3</sub>pyra], using mole ratio scale. Curves show model calculations based on Eq. (9), with parameters  $\Delta h_{\text{chem}}^0 = -42800$  J/mol,  $\Delta s_{\text{chem}}^0 = -122$  J/(mol K),  $\Delta h_{\text{phys}}^0 = -12000$  J/mol,  $\Delta s_{\text{phys}}^0 = -71$  J/(mol K),  $C_1 = 0.94$ , and  $C_2 = 0.0005$ .

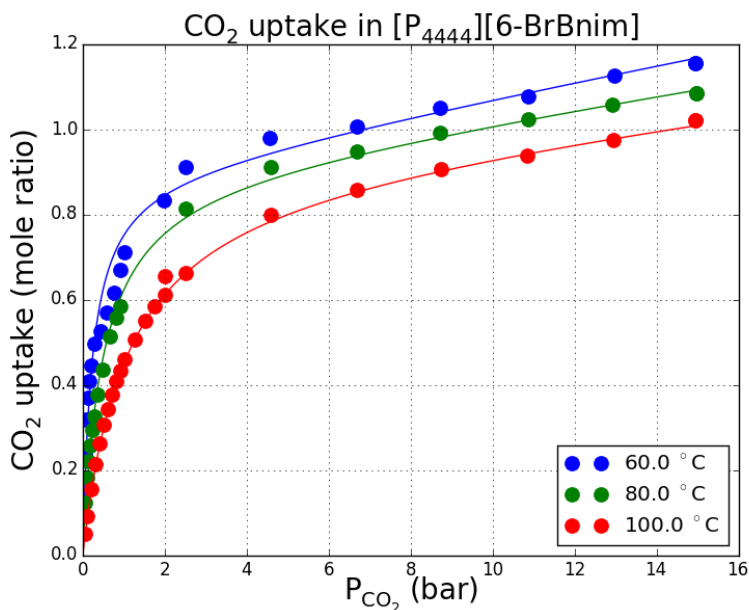


Figure 5. Experimental uptake data<sup>89</sup> for  $[P_{4444}][6\text{-BrBnim}]$ , using mole ratio scale. Curves show calculations based on Eq. (9), with parameters  $\Delta h_{\text{chem}}^0 = -45300$  J/mol,  $\Delta s_{\text{chem}}^0 = -122$  J/(mol K),  $\Delta h_{\text{phys}}^0 = -12700$  J/mol,  $\Delta s_{\text{phys}}^0 = -71$  J/(mol K),  $C_1 = 0.93$ , and  $C_2 = 0.0003$ .

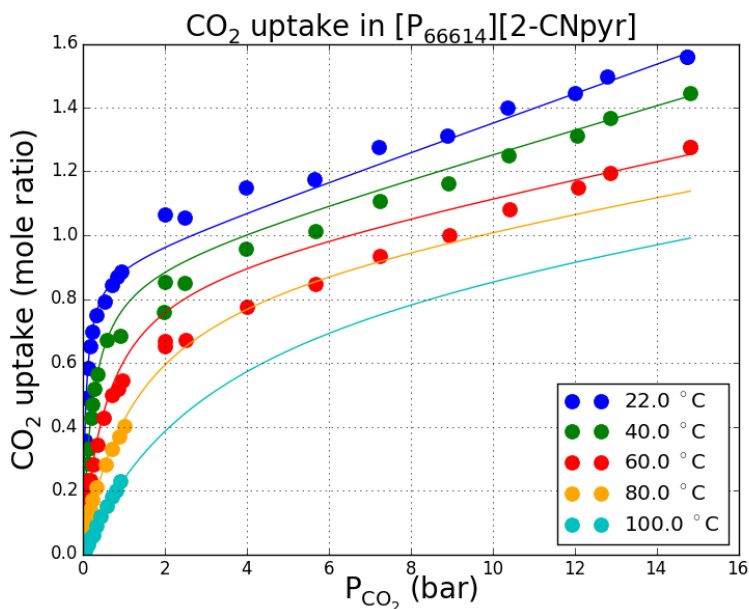


Figure 6. Experimental uptake data<sup>46,89</sup> for  $[P_{66614}][2\text{-CNpyr}]$ , using mole ratio scale. Curves show model calculations based on Eq. (9), with parameters  $\Delta h_{\text{chem}}^0 = -45000$  J/mol,  $\Delta s_{\text{chem}}^0 = -130$  J/(mol K),  $\Delta h_{\text{phys}}^0 = -13200$  J/mol,  $\Delta s_{\text{phys}}^0 = -70$  J/(mol K),  $C_1 = 0.92$ , and  $C_2 = 0.0005$ .

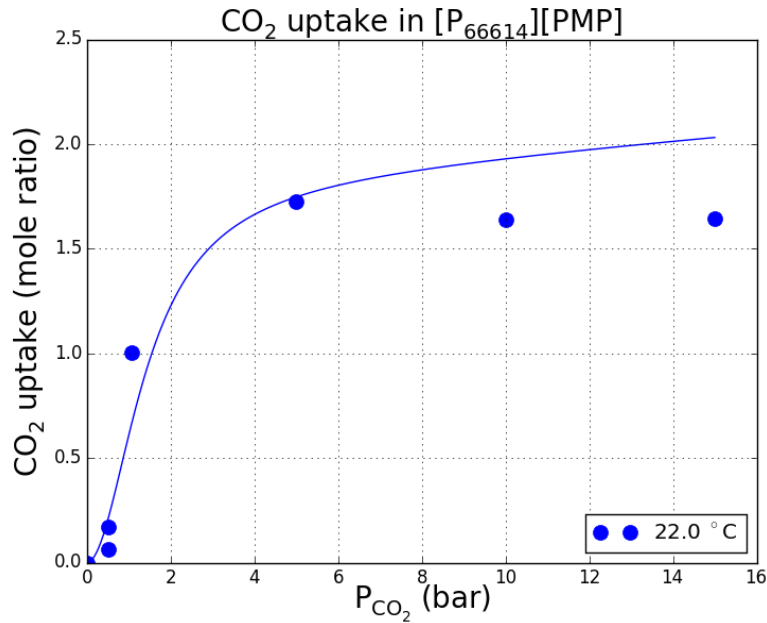


Figure 7. Experimental uptake data for  $[\text{P}_{66614}][\text{PMP}]$  at 295.15 K, using mole ratio scale. Curves show model calculations based on Eq. (12), with parameters  $\Delta h_{\text{chem},1}^0 = -20000$  J/mol,  $\Delta h_{\text{chem},2}^0 = -55000$  J/mol,  $\Delta s_{\text{chem},1}^0 = \Delta s_{\text{chem},2}^0 = -130$  J/(mol K),  $\Delta h_{\text{phys}}^0 = -10000$  J/mol,  $\Delta s_{\text{phys}}^0 = -68$  J/(mol K), and  $X_{\text{chem}}^0 = 0.9$ . See text for additional discussion of data.

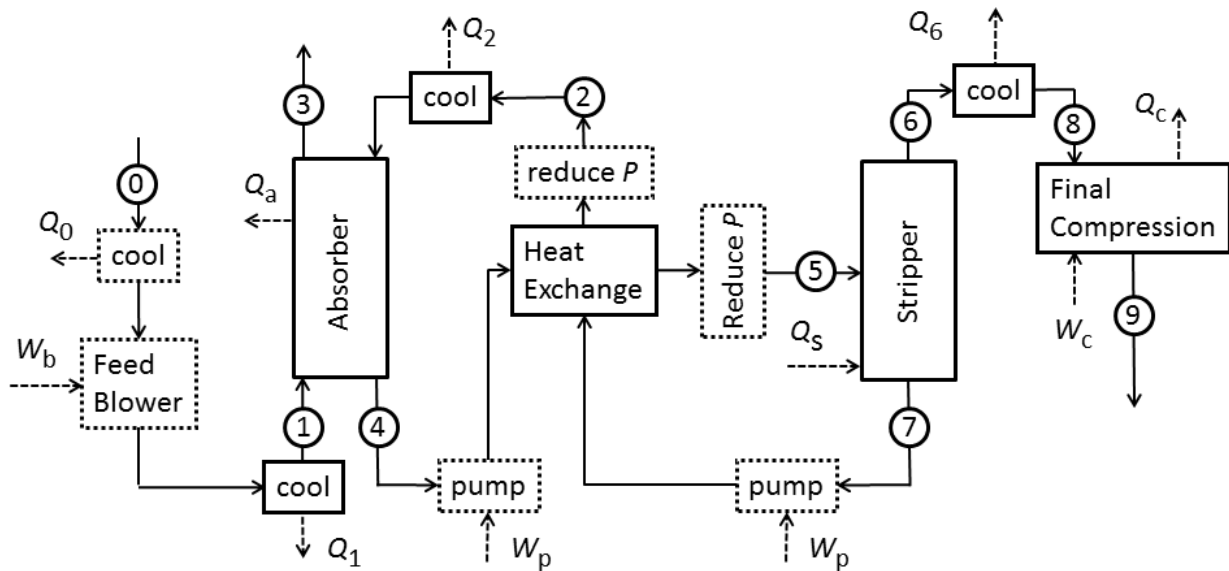


Figure 8. Block diagram for simple process model. Dotted blocks indicate units that may not be used. See detailed discussion in text.

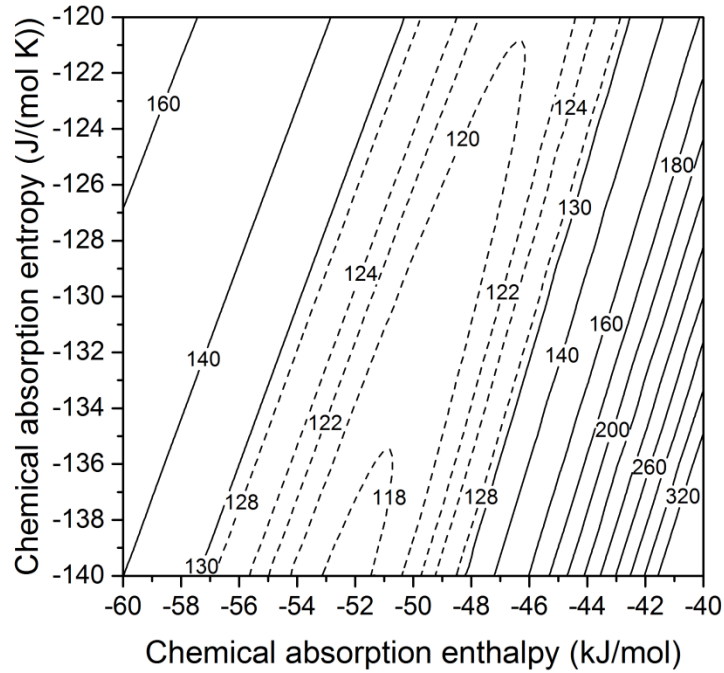


Figure 9. Variation in the optimal parasitic energy  $E^*$  (MWe) with the chemical absorption enthalpy,  $\Delta h_{\text{chem}}$ , and entropy,  $\Delta s_{\text{chem}}$ , with other sensitivity parameters held at their base values (Table 2) and for PC flue gas (Table 1). Contour spacing is 2 MWe for  $E^* < 130$  MWe and 20 MWe for  $E^* > 140$  MWe.

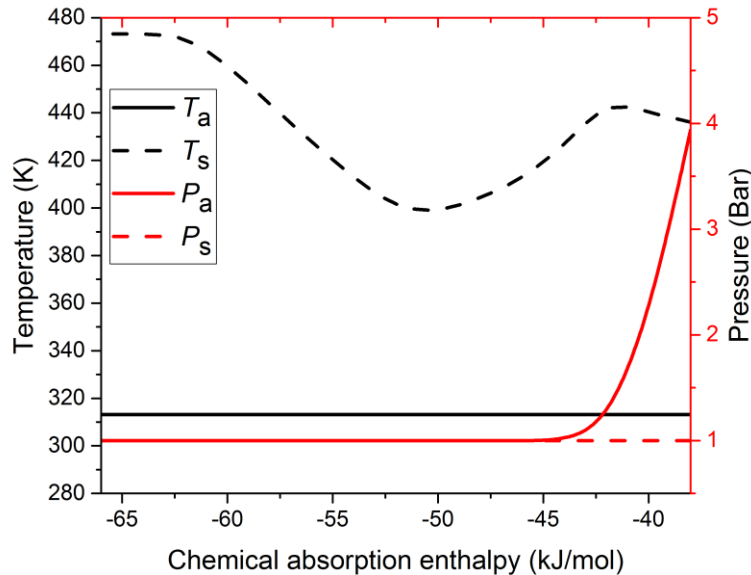


Figure 10. Optimal values of the absorber and stripper conditions vs.  $\Delta h_{\text{chem}}$ , for the case of  $\Delta s_{\text{chem}} = -130$  J/(mol K), with other sensitivity parameters held at their base values (Table 2) and for PC flue gas (Table 1).

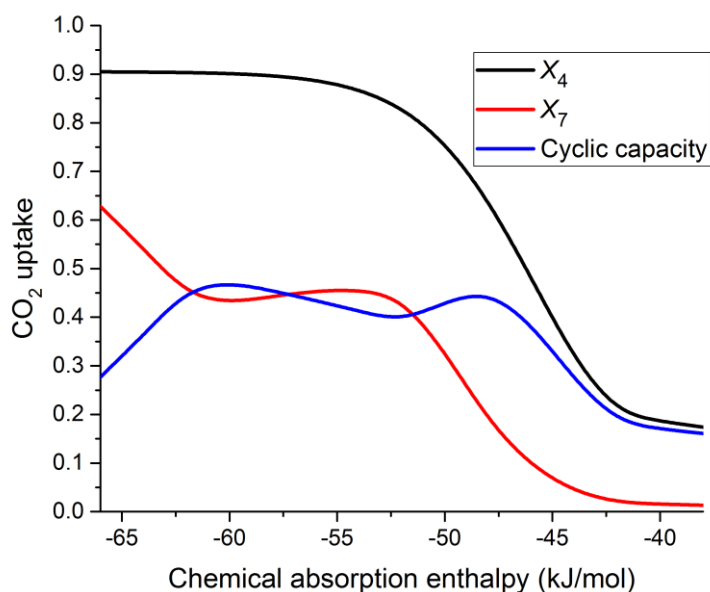


Figure 11. Optimized rich ( $X_4$ ) and lean ( $X_7$ ) stream uptakes and cyclic capacity ( $X_4 - X_7$ ) vs.  $\Delta h_{\text{chem}}$  for  $\Delta s_{\text{chem}} = -130 \text{ J}/(\text{mol K})$ , with other sensitivity parameters held at their base values (Table 2) and for PC flue gas (Table 1).

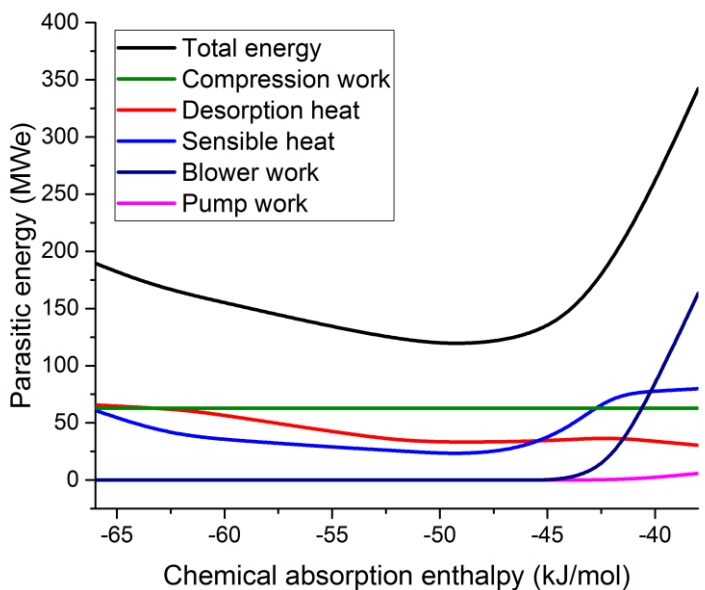


Figure 12. Optimized parasitic energy  $E^*$  and its components vs.  $\Delta h_{\text{chem}}$  for  $\Delta s_{\text{chem}} = -130 \text{ J}/(\text{mol K})$ , with other sensitivity parameters held at their base values (Table 2) and for PC flue gas (Table 1).

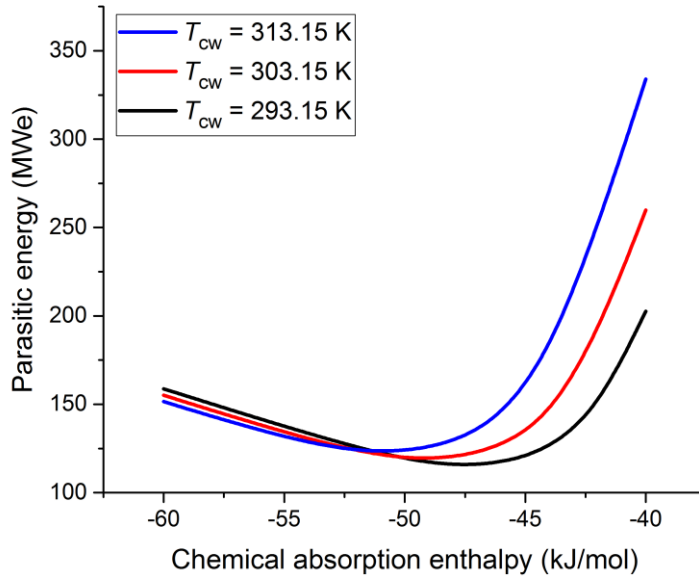


Figure 13. Sensitivity of optimized parasitic energy  $E^*$  with respect to cooling water temperature  $T_{cw}$  for  $\Delta s_{chem} = -130$  J/(mol K), with other sensitivity parameters held at their base values (Table 2) and for PC flue gas (Table 1).

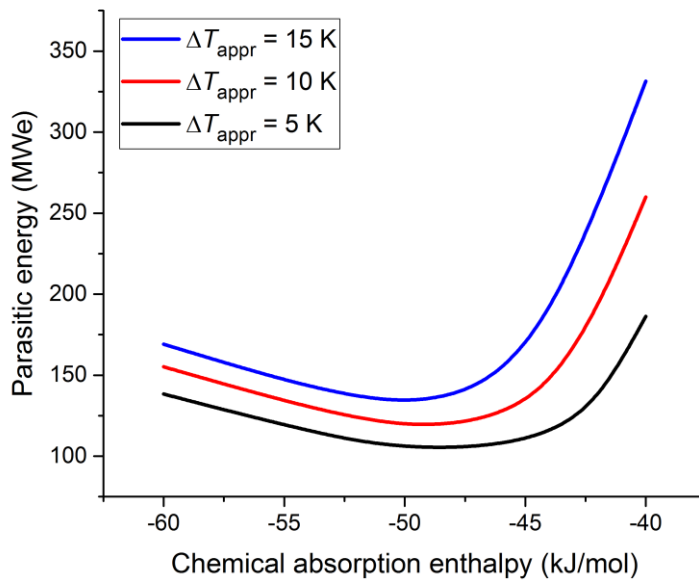


Figure 14. Sensitivity of optimized parasitic energy  $E^*$  with respect to minimum approach temperature  $\Delta T_{appr}$  for  $\Delta s_{chem} = -130$  J/(mol K), with other sensitivity parameters held at their base values (Table 2) and for PC flue gas (Table 1).

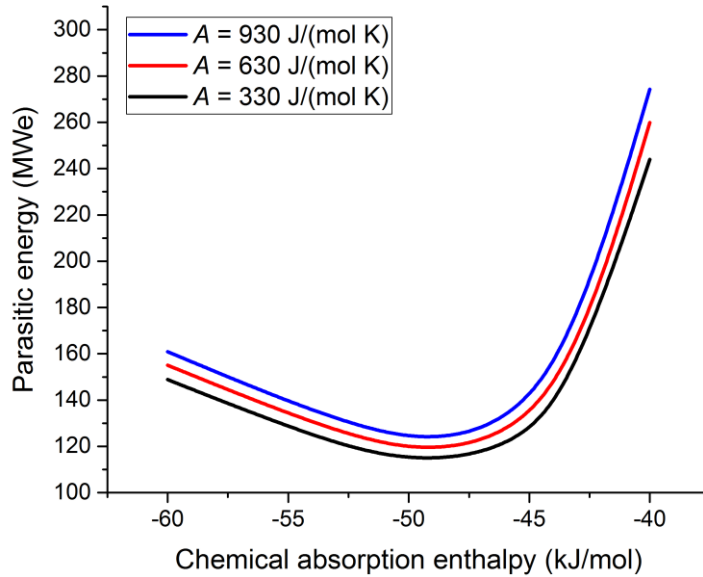


Figure 15. Sensitivity of optimized parasitic energy  $E^*$  with respect to the base heat capacity parameter  $A$  for  $\Delta s_{\text{chem}} = -130$  J/(mol K), with other sensitivity parameters held at their base values (Table 2) and for PC flue gas (Table 1).

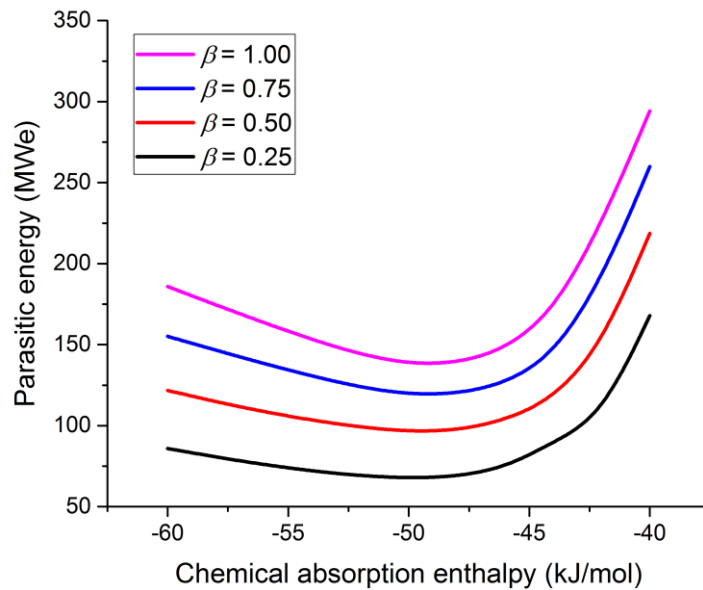


Figure 16. Sensitivity of optimized parasitic energy  $E^*$  with respect to the process integration factor  $\beta$  for  $\Delta s_{\text{chem}} = -130$  J/(mol K), with other sensitivity parameters held at their base values (Table 2) and for PC flue gas (Table 1).

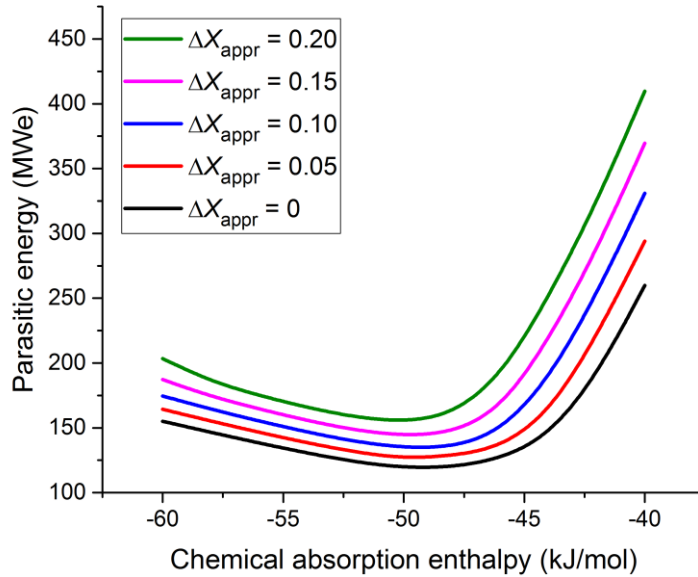


Figure 17. Sensitivity of optimized parasitic energy  $E^*$  with respect to  $\Delta X_{\text{appr}}$ , the approach to saturation of the rich  $\text{CO}_2$ -rich stream leaving the absorber, for  $\Delta s_{\text{chem}} = -130 \text{ J}/(\text{mol K})$ , with other sensitivity parameters held at their base values (Table 2) and for PC flue gas (Table 1).

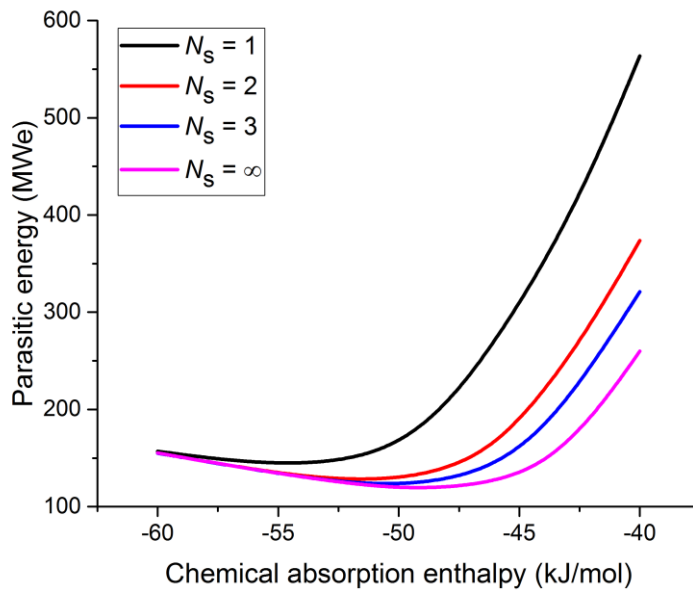


Figure 18. Sensitivity of optimized parasitic energy  $E^*$  with respect to the number of ideal stages  $N_s$  for  $\Delta s_{\text{chem}} = -130 \text{ J}/(\text{mol K})$ , with other sensitivity parameters held at their base values (Table 2) and for PC flue gas (Table 1).

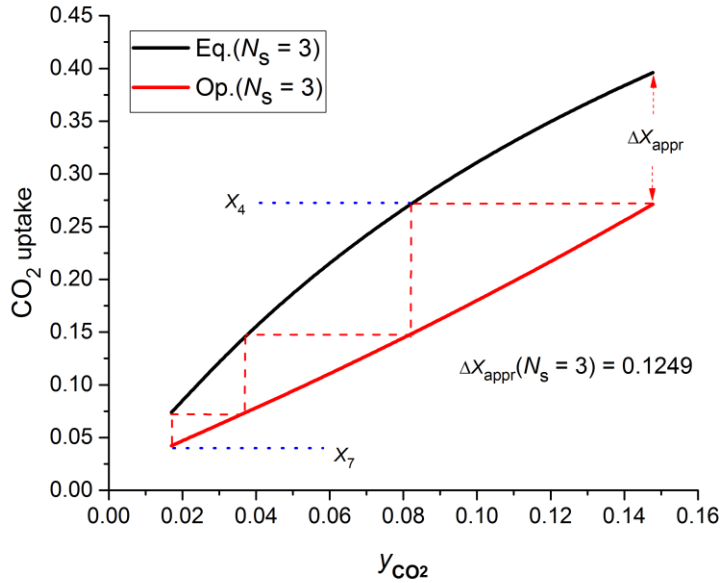


Figure 19. Optimized absorber operating diagram for  $N_s = 3$ , showing equilibrium curve and operating curve, for  $\Delta h_{\text{chem}} = -45$  kJ/mol and  $\Delta s_{\text{chem}} = -130$  J/(mol K), with other sensitivity parameters held at their base values (Table 2) and for PC flue gas (Table 1). The optimal absorber conditions for this case are  $T_a = 313.15$  K and  $P_a = 1$  bar.

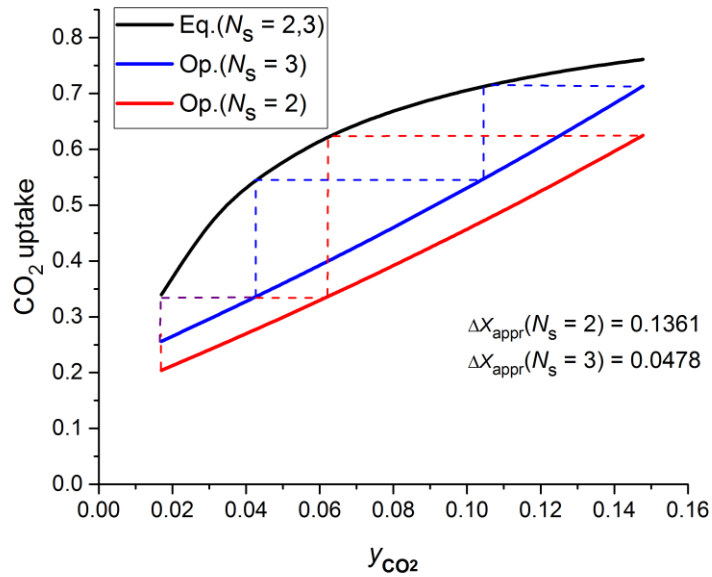


Figure 20. Optimized absorber operating diagrams for  $N_s = 2$  and 3, showing equilibrium curve and operating curves, for  $\Delta h_{\text{chem}} = -50$  kJ/mol and  $\Delta s_{\text{chem}} = -130$  J/(mol K), with other sensitivity parameters held at their base values (Table 2) and for PC flue gas (Table 1). The optimal absorber conditions for this case are  $T_a = 313.15$  K and  $P_a = 1$  bar.

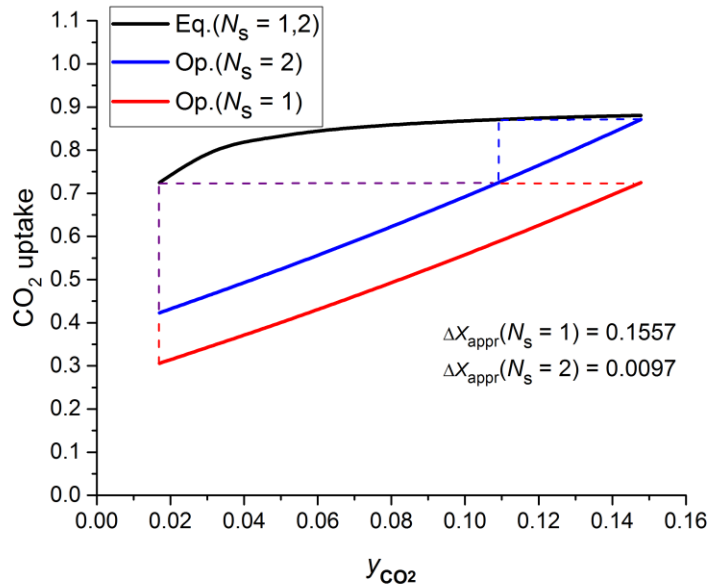


Figure 21. Optimized absorber operating diagrams for  $N_s = 1$  and 2, showing equilibrium curve and operating curves, for  $\Delta h_{\text{chem}} = -55$  kJ/mol and  $\Delta s_{\text{chem}} = -130$  J/(mol K), with other sensitivity parameters held at their base values (Table 2) and for PC flue gas (Table 1). The optimal absorber conditions for this case are  $T_a = 313.15$  K and  $P_a = 1$  bar.

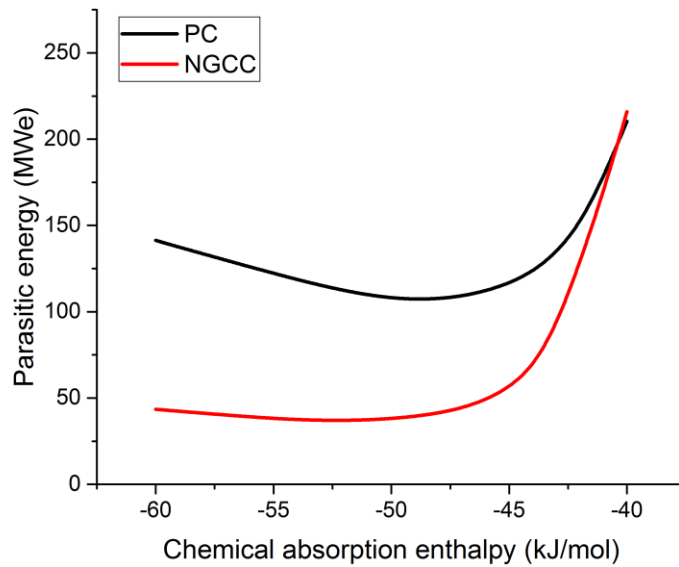


Figure 22. Optimized parasitic energy  $E^*$  vs.  $\Delta h_{\text{chem}}$  for PC and NGCC flue gas with  $\Delta s_{\text{chem}} = -130$  J/(mol K), two ideal absorber stages ( $N_s = 2$ ), best-case values of other process parameters ( $T_{\text{cw}} = 293.15$  K,  $\Delta T_{\text{appr}} = 5$  K), and other sensitivity parameters held at their base values (Table 2).

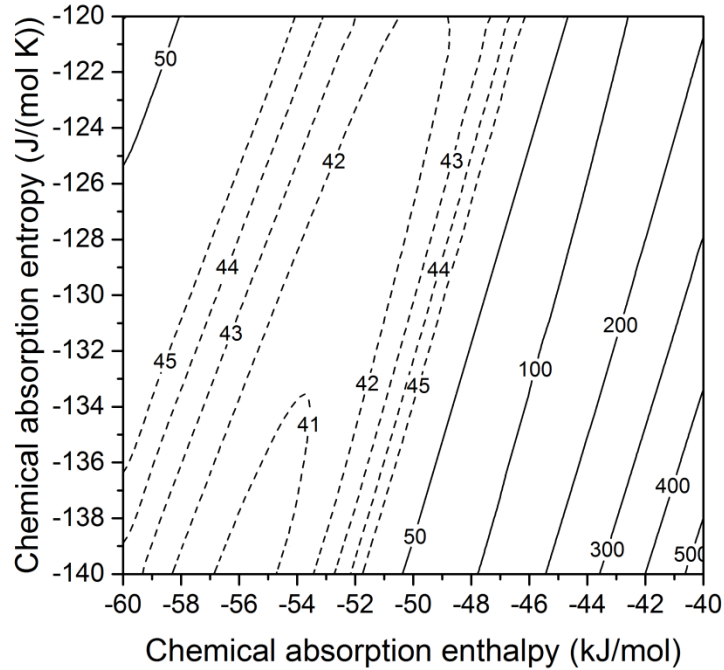


Figure 23. Variation in the optimal parasitic energy  $E^*$  (MWe) with the chemical absorption enthalpy,  $\Delta h_{\text{chem}}$ , and entropy,  $\Delta s_{\text{chem}}$ , with other sensitivity parameters held at their base values (Table 2) and for NGCC flue gas (Table 1). Contour spacing is 1 MWe for  $E^* < 45$  MWe and 100 MWe for  $E^* > 50$  MWe.

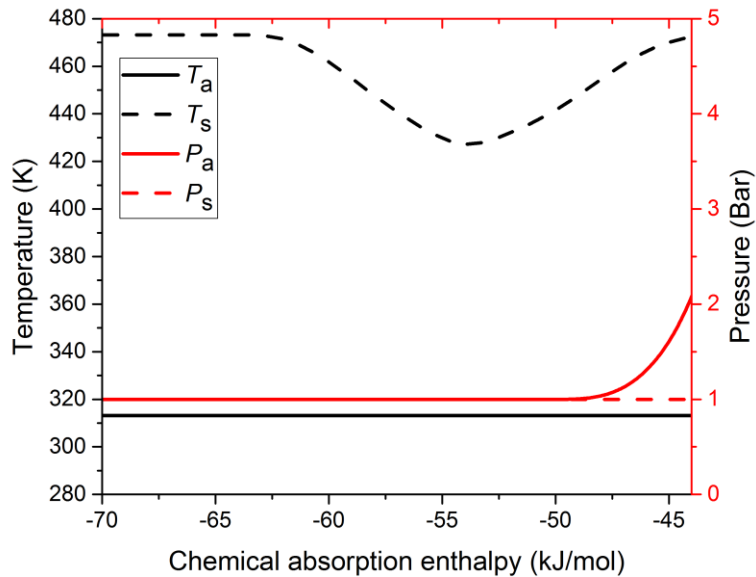


Figure 24. Optimal values of the absorber and stripper conditions vs.  $\Delta h_{\text{chem}}$ , for the case of  $\Delta s_{\text{chem}} = -130$  J/(mol K), with other sensitivity parameters held at their base values (Table 2) and for NGCC flue gas (Table 1).

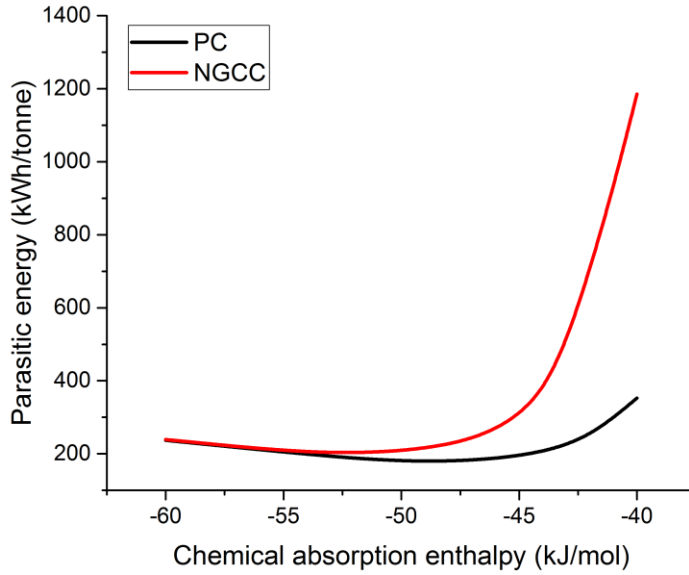


Figure 25. Optimized parasitic energy per metric ton of CO<sub>2</sub> captured vs.  $\Delta h_{\text{chem}}$  for PC and NGCC flue gas with  $\Delta s_{\text{chem}} = -130$  J/(mol K), two ideal absorber stages ( $N_s = 2$ ), best-case values of other process parameters ( $T_{\text{cw}} = 293.15$  K,  $\Delta T_{\text{appr}} = 5$  K), and other sensitivity parameters held at their base values (Table 2).

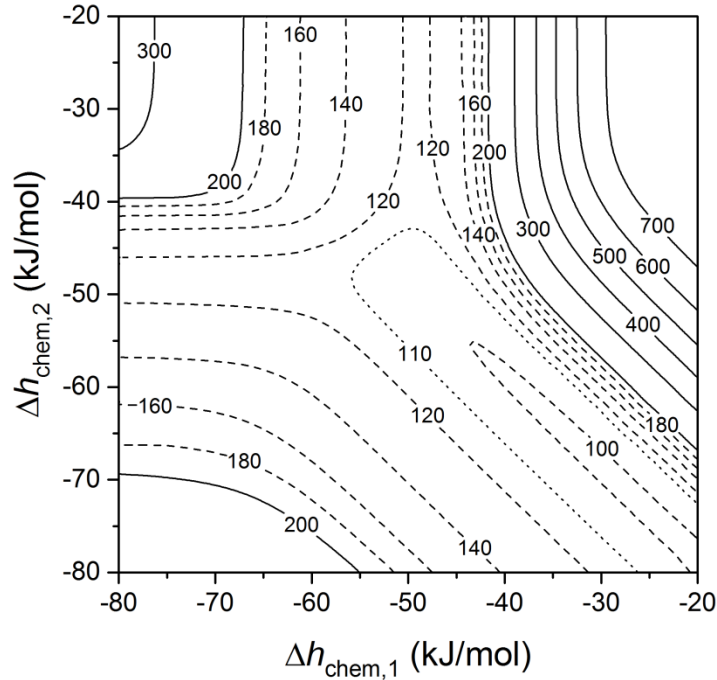


Figure 26. Variation in the optimal parasitic energy  $E^*$  (MWe) with  $\Delta h_{\text{chem},1}$  and  $\Delta h_{\text{chem},2}$  for two-site AHA and PC flue gas (Table 1), with  $\Delta s_{\text{chem},1} = \Delta s_{\text{chem},2} = -130$  J/(mol K) and other sensitivity parameters held at their base values (Table 2).

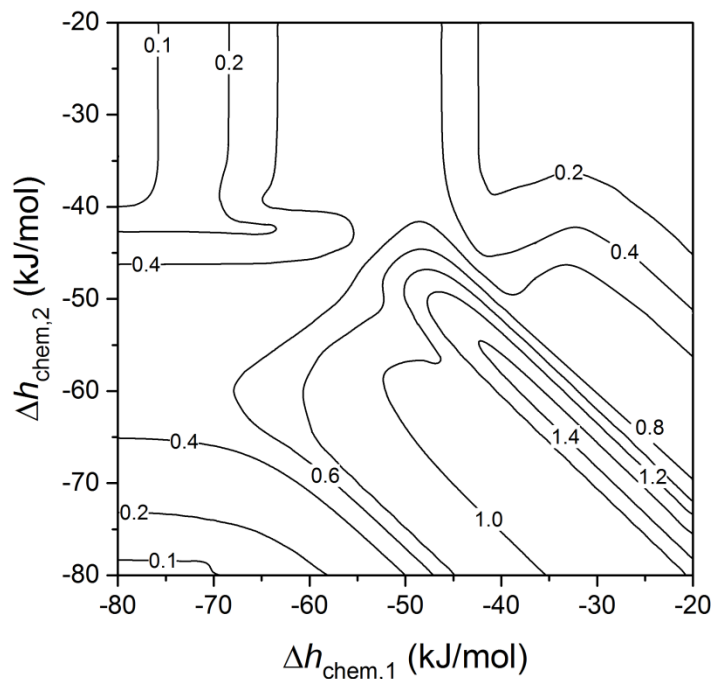


Figure 27. Variation in the optimal cyclic capacity with  $\Delta h_{\text{chem},1}$  and  $\Delta h_{\text{chem},2}$  for two-site AHA and PC flue gas (Table 1), with  $\Delta s_{\text{chem},1} = \Delta s_{\text{chem},2} = -130 \text{ J}/(\text{mol K})$  and other sensitivity parameters held at their base values (Table 2).

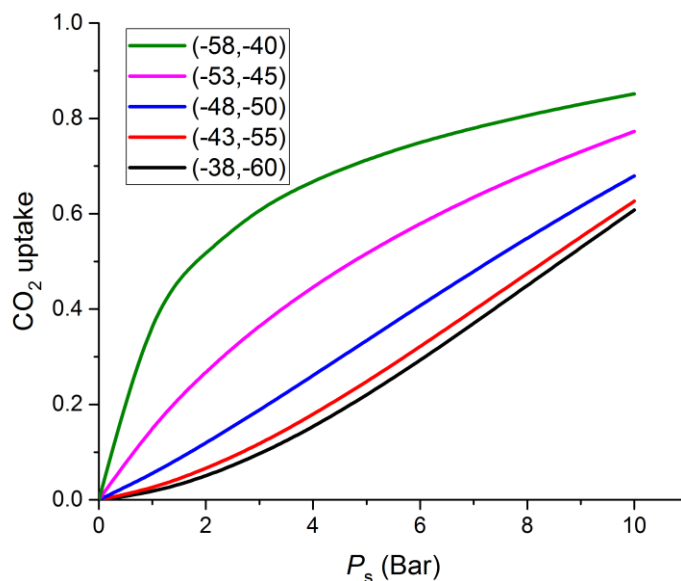


Figure 28. Uptake isotherms at stripper temperature of 455 K, for several values of  $(\Delta h_{\text{chem},1}, \Delta h_{\text{chem},2})$  kJ/mol on the line  $\Delta h_{\text{chem},1} + \Delta h_{\text{chem},2} = -98 \text{ kJ/mol}$ . See text for discussion.

For Table of Contents Only

